Dendritic crystal growth for weak undercooling

M. D. Kunka, M. R. Foster, and S. Tanveer
The Ohio State University, Columbus, Ohio 43210

Through an asymptotic expansion for small undercooling (i.e., Péclet number $P \ll 1$), different regions of a two-dimensional evolving dendrite in a one-sided model are identified, when the dendrite shape is initially parabolic in the far field. There is an $o(P^{-1})$ tip region (region I) where the temperature field is a Laplacian with an appropriate matching condition to the far field. For deviations to an Ivantsov field that are initially limited to this region, it is shown to be consistent to assume that the Ivantsov solution is asymptotically valid in the far-field asymptotic regions when $t \ll P^{-1}$. Within this interval of time, we consider the dynamics in region I through an integro-differential equation derived from a conformal mapping formulation, where the upper-half ζ plane is mapped to the exterior of the dendrite. It is shown that a linear analysis of an initially localized disturbance fails to remain localized later in time. Instead, it results in a partially wavy interface where the waviness has a sharp leading edge. This feature is shown to be related to the Stokes phenomenon associated with the inner equation around an initial complex singularity in the lower-half ζ plane, as it advects into the upper-half ζ plane. The specific linear growth rate is shown to be consistent with prior results of Barber, Barbieri, and Langer [Phys. Rev. A **36**, 3340 (1987)], though not with Caroli *et al.* [J. Phys. (Paris) **48**, 1423 (1987)]. The results do not depend crucially on the nature of initial disturbance or the singularity in the lower-half complex ζ plane that is used to represent such a disturbance. However, nonlinear effects are shown to cause important changes in the prediction for both qualitative and quantitative aspects. This understanding is advanced by considering the dynamics of singularities in the lower-half complex ζ plane. We also present many features of the zero-surface-energy dynamics including tip splitting, sidebranching, as well as cusp formation. We also present a scenario for dendrite sidebranch coarsening in terms of the motion of complex singularities. [S1063-651X(97)05405-6]

PACS number(s): 81.10.Aj

I. INTRODUCTION

Dendritic crystal growth has been a subject of continued interest to physicists, metallurgists, as well as mathematicians. The most common example of such a growth is the well-known ice crystal. From a physicist's perspective, dendrites constitute a relatively simple but important problem of pattern formation in nonequilibrium growth [1–3]. In metallurgy, dendrites are common to crystal formation in the manufacture of alloy castings, metal ingots, and weldments [4]. They form in the process of directional solidification of a binary alloy when the growth rate exceeds some critical value. Unlike the case of the crystallization of a pure material, where growth is determined by diffusion of the temperature field, the dendrites in directional solidification are controlled by the mass diffusion of one binary component relative to another. The resulting solid is rich in microstructures that ultimately control many of the properties of the finished product. A fuller understanding of dendrite formation is considered vital to controlling this technologically important process. From a mathematician's perspective, dendrite formation is an extended version of the classical one-dimensional Stefan problem: a free boundary problem where the domain has to be determined as part of the solution. The most common and simple mathematical model that is believed to be relevant to dendrite formation consists of a linear diffusion equation describing the diffusion of heat or solute, as the case may be. A far-field condition on temperature or concentration is specified as well in accordance with the experimental condition. Additionally, to make the problem

well defined, one specifies two interfacial boundary conditions: One is the Gibbs-Thomson boundary condition that accounts for lowering of the melting temperature by curvature or kinetic effects, while the other follows from a balance of heat or mass at the interface, where solidification releases latent heat. The Gibbs-Thomson relation assumes a local thermodynamic equilibrium, which is appropriate since the thermodynamic time scale of relaxation is usually much shorter than the time scale of diffusion. Further, except in cases where the growth rate is very high, kinetic effects on the melting temperature are small and hence ignored. In any case, the additional boundary condition on the interface (two instead of one) determines the evolution of the free surface boundary.

The relevance of the above model to experimental observations is not definitely clear. Many effects that are believed to be small have been ignored; yet anisotropy in the surface energy relation, even though very small for some crystals, is crucial to theoretical predictions, at least for one theory based on the above model (see review articles [1–3]). Experimental support for such a preeminent role of anisotropy, at least for tip characteristics, does not seem to exist [4]. To understand if such a discrepancy arises from inherent limitations of the model or from the additional assumptions made in the theory, one must understand the full mathematical implications of the model equations, but that understanding has yet to emerge.

A steadily moving planar front is unstable due to the well-known Mullins-Sekerka instability [5]. Experimental observations of the dendrite's parabolic tip motivated the search

for steady solutions that are approximately parabolic. Neglecting the Gibbs-Thomson lowering of melting temperature, and for a specific choice of ''undercooling'' at infinity, Ivantsov [6] found an exact solution for a steadily growing needle crystal in the form of a parabola, in two dimensions, and an axisymmetric paraboloid in three dimensions. The solutions were later extended to elliptical paraboloids by Horvay and Cahn [7]. Since capillary effects are ignored in these results, there is no intrinsic length scale and so it is not surprising that these solutions do not give a unique determination of the tip radius. For a given undercooling and fixed material constants, only the product of the tip radius and velocity is determined from these solutions. Experimentally, on the other hand, both the tip radius and tip speed are determined uniquely for given conditions [8]. Although the observed product of the tip radius and tip velocity is in rough agreement with theory, the agreement is not very good [9] presumably due to those factors not incorporated in the model described above.

Following Ivantsov's seminal work, much attention was paid to the effect of surface energy in removing the degeneracy in the steady solution. Much of the earlier work utilizes *ad hoc* hypotheses. The marginal stability hypothesis [10], which requires that the selected tip radius must be such that the tip is neutrally stable to disturbances, is an example and it leads to a determination of the product of the square of the tip radius and tip velocity. When combined with the Ivantsov relation, both the tip radius and velocity are then uniquely given. This theory does not necessitate the inclusion of crystalline anisotropy and predictions can be made in two as well as three dimensions. Despite the relative simplicity of this theory and reasonable agreement of some prediction with experiment, no tenable mathematical justification for the marginal stability hypothesis exists [4].

In the 1980s, following progress on model problems [11], the ''microscopic solvability'' criterion emerged, to describe the effects of capillarity on the Ivantsov steady-state solutions [12]. Numerous numerical and analytical evidences for two- and three-dimensional dendrites suggest that the sole inclusion of isotropic surface energy does not give a steady-state needle crystal that asymptotically approaches an Ivantsov solution in the far field. This apparent lack of regularity in the perturbations of the Ivantsov solution for arbitrarily small isotropic surface energy is mathematically reflected in exponentially small terms in the asymptotic expansion. When surface energy anisotropy is modeled by a fourfold anisotropic term in two dimensions, a discrete set of steady states exists, only one of which is linearly stable [13]. Thus a unique steady-state tip radius and tip velocity are predicted. In addition, for small surface energy, the steady-state correction to the Ivantsov parabola due to surface energy remains small everywhere. However, in three dimensions, there has been recent work [14] that suggests that surface energy causes large nonaxisymmetric deviations from the Ivantsov paraboloid far from a tip that is approximately parabolic. It is unclear at this time if the large nonaxisymmetric deviations observed in experiment cannot be alternately explained by the existence of nonaxisymmetric zero surface energy solutions.

While the evidence for steady-state selection in the context of the theoretical model equations is firm in two dimensions, the relevance of any theoretical steady-state solution to the observed dendrite is far from evident. Dendrites are hardly steady, except perhaps for a small region around the tip. The microscopic solvability theory explains the dendritic features as resulting from the convective instability of tip disturbances [15–18] advecting along the sides of the assumed steady needle crystal, though the nonlinear stages of the growing disturbance have not been addressed. It is unclear if results based on linearization about a global steady state are not too restrictive in ruling out other qualitatively different phenomena associated with the full, time-evolving problem. As an example, a time-dependent dendritic state that is steady only near the tip might exist in the absence of anisotropy.

The advent of powerful computers has led to a new and important theoretical tool. Indeed numerical simulations are now possible that make it possible to include many nonlinear features of of a time-evolving two-dimensional dendrite. Numerical calculations for the dendrite, either for a sharp interface with a Gibbs-Thomson interface condition [19–23] or in the context of a phase-field calculation [24–30] suggest that the product of tip velocity and radius squared is consistent with microscopic solvability, even when the dendrite or finger is evolving in time. (See the mathematically similar feature in the problem of viscous fingering with anisotropic surface energy [31].) The results lend support to the premises of microscopic solvability, though they do not explain the physical mechanisms whereby a localized steady-state tip condition is possible even while the bulk of the dendrite is evolving in time. Further, it remains unclear how the amplification of localized disturbances superposed on a steady dendrite compare with that of localized disturbances on an arbitrary, time-evolving state. In particular, phase field model calculations are reliable indicators of the limiting sharp interface features only when the width of the transition zone is comparable to or smaller than the capillary length scale. This limitation constrains the investigation of the small capillary effect limit, which is the purpose of the current investigation. In general, numerical calculations, by themselves, appear to be unsuitable in providing scaling dependences on parameters.

Although the theory of dendritic crystal growth has seen significant development, there is a lack of sound theoretical understanding of observed dynamical features of a dendrite and how apparently small effects of surface energy (the capillary length is of the order of micrometers in many materials) influence global features of a time-evolving dendritic shape. As far as we know, all analytical investigations thus far have been based on some kind of linearization about a steady base state. In this paper we introduce a systematic investigation of the fully nonlinear dendritic evolution, within an analytical framework. In particular, we address the mathematical origin of the observed chaotic dependence of specific dendrite shapes on initial conditions, the unexpected observation that, in many situations, each dendrite grows relatively independently of its neighbors, and the fact that the growth process is apparently self-similar in all scales up to the capillary cutoff scale. We also address, within an analytical framework, how arbitrarily small surface energy dynamically selects tip radius and speed relations, without assumptions on a global steady state, in accordance with

microscopic solvability, even as the rest of the dendrite is unsteady. Further, for a specific set of initial conditions, we predict the time over which dynamic selection of the tip relation occurs.

In a sequence of three papers, we plan to examine the time evolution of a two-dimensional dendrite in a weakly undercooled melt, using a one-sided model; small undercooling means that the Péclet number is small. Our focus is almost exclusively on the case for which the surface energy effects are appropriately small. For a dendrite that is roughly parabolic, surface energy effects weaken with distance from the tip, due to decreasing curvature. Therefore, the small-surface-energy limit has obvious relevance. Further, accurate numerical simulation of a time-evolving dendrite in the small-surface-energy limit is difficult because of the need to resolve fine scales in both space and time. Our objective is to combine analytical and numerical methods to shed light on the dynamics in this limit of small surface energy. Although a three-dimensional model is faithful to experimental reality, many theoretical issues related to the model, e.g., tip characteristics and sidebranching, also arise in the more mathematically tractable two-dimensional problem. The hope is that theoretical understandings gained will carry over to three dimensions, at least in a qualitative sense. For the growth of a crystal in a melt, a two-sided symmetric model is more relevant since the temperature diffusion constant in the solid is not generally all that different from that in the melt. Nonetheless, a one-sided model can be relevant when growth is controlled by solute diffusion since the diffusion in the solid is small in many instances. Further, numerical calculations suggest that the qualitative features for one-sided and two-sided symmetric models are about the same, at least in the context of a steadily growing dendrite. However, given the sensitivity of the evolving dendrite to small effects, it is conceivable that the two-sided model can be quantitatively, if not qualitatively, different.

The present paper is the first part of the sequence of papers noted and it concerns the determination of asymptotic equations for small Péclet number (weak undercooling), the linear growth of small scale disturbances for small surface energy, the nonlinear zero-surface-energy dynamics of initially specified complex singularities in the lower-half plane, and their connection to interfacial evolution. It is important to make clear this connection to the detailed nonlinear analysis of the zero-surface-energy dynamics presented in Sec. IV onward. Therefore, in Sec. III, we present an illustrative example of the singularity motion for the much simpler linearized dynamics, together with its relation to the growth and dispersion of small disturbances superposed on an Ivantsov solution. We plan to follow with two papers that further explore the understanding of this process in the complex plane.

The outline of the present paper is as follows. In Sec. II we construct a formal asymptotic expansion for weak undercooling (small Péclet number P) and determine where an assumed regular expansion ceases to be consistent. For a dendrite that is initially Ivantsov-like in the far field, we show that there are three asymptotic regions with different governing equations and scales—where time is measured in units of a/U, where a, U denote the tip radius and velocity of the corresponding Ivantsov solution. For an $O(1)$ region around the tip, ''region I,'' to the leading order in Péclet

number, the temperature obeys Laplace's equation with boundary and far-field conditions very similar to those for unstable viscous fingering in a Hele-Shaw cell [2,3]. When initial shape deviations from an Ivantsov parabola (not necessarily small or localized) are confined to region I, we find that it is consistent to assume that in other regions the temperature and interfacial shape remain that for the Ivantsov solution, as long as the time $t \ll P^{-1}$. For t satisfying this constraint, we investigate in Sec. III the growth and advection of initially localized disturbances superposed on an arbitrary time-evolving state. The results of the linearized analysis are in conformity with previous analytical results of Barber, Barbieri, and Langer [16], but in disagreement with Caroli, Caroli, and Roulet [18]. In particular, we find that linear analysis predicts that an initially localized disturbance fails to remain localized—an observation overlooked in previous work. By considering analytic continuation into a complex plane, we can understand more fully the meaning of the wave-packet analyses that have been previously done.

The complex plane analysis is also suitable if we like to understand small surface energy effects in a perturbation procedure about the zero-surface-energy dynamics, which is well posed in the extended complex plane [32,34,37], but ill posed in the real domain. This perturbation procedure seems to be the only practical option for the fully nonlinear problem, which is the main focus of this and the companion papers. The linear results on the connection of complex singularity motion and interfacial dynamics motivates the study of the complex dynamics for the fully nonlinear problem.

As a first step, it is necessary to study the zero-surface-energy dynamics in the extended complex domain, though not all such solutions can be the limit solutions as surface energy shrinks to zero—as we know from earlier work in the analogous mathematical problem of viscous fingering in a Hele-Shaw cell [34–36]. To understand and predict possible differences, we are naturally led in Sec. IV to investigating fully nonlinear dynamics in the extended complex plane, where the zero-surface-energy equations are in fact well posed [37]. The complex plane specification of initial conditions, while apparently artificial from the viewpoint of an experimentalist who is in a position to determine only the initial interfacial shape to a finite precision, has the theoretical advantage of removing all sensitivity of the dynamics to initial conditions. In this formulation, the actual results of an experiment are to be understood by studying a random ensemble of initial conditions in the complex plane, subject to the constraint that the corresponding initial shapes for all these initial conditions differ only by errors of measurement. In terms of complex zero-surface-energy dynamics involving certain singularities, we also present a possible mechanism for nonlinear coarsening of the side-branches.

Our approach is restricted to analytic initial interfacial shapes, for which the analytic continuation of the conformal map $z(\zeta, t)$ to the lower half ζ plane includes only isolated singularities of certain types. While this is not generic, we proceed with the expectation that the aggregate features of the observed dynamics are not sensitive to the precise nature of singularities.

In this paper we restrict discussion to the various features of the *zero-surface-energy* dynamics in the complex plane and the corresponding features observed at the interface, and
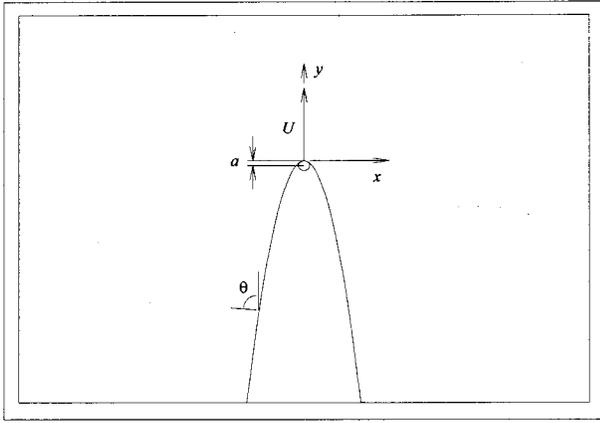
FIG. 1. Problem domain: x,y, crystal-frame coordinates; θ, angle between interface normal and y axis.

as such this paper is the precursor to the two future papers, which address the differences between the zero-surface-energy dynamics worked out here and actual dendritic dynamics in the limit as surface energy tends to zero.

II. ONE-SIDED MODEL EQUATIONS

For purposes of the analysis to follow, we introduce the following nondimensionalization. Temperature is measured in units of L/c_p, where L is the the latent heat and c_p the specific heat capacity. Lengths are measured in units of the tip radius a for the Ivantsov parabola that describes the asymptotic shape of the dendrite far from the tip. (Notice that a need not be the actual tip radius.) Velocities are measured in units of U, where U is such that the Péclet number $P = Ua/2D$ satisfies the Ivantsov relation between P and dimensionless undercooling $\Delta = (c_p/L)(T_m - T_\infty)$. [See Eq. (2.14) below.] Here D is the diffusivity in the melt and T_m and T_∞ are the dimensional melting temperatures for a flat interface and the specified temperature at infinity, respectively.

With this nondimensionalization, in the frame where an Ivantsov parabolic interface would have been stationary, the dimensionless temperature variable T, with the melting temperature of a flat interface subtracted before nondimensionalization, satisfies

$$2P \frac{\partial T}{\partial t} = 2P \frac{\partial T}{\partial y} + \nabla^2 T, \qquad (2.1)$$

exterior to the interface shown in Fig. 1. The condition at infinity that determines T for a specified the undercooling is

$$T \rightarrow -\Delta \quad \text{as } y \rightarrow \infty, \qquad (2.2)$$

while the conservation of heat through the interface requires

$$\frac{\partial T}{\partial n} = -2P[v_n + \cos(\theta)] \quad \text{on } y = y_i(x,t), \qquad (2.3)$$

where v_n is the normal component of the interface motion and θ is the angle between the interface and the y axis. The assumption of local thermodynamic equilibrium implies the
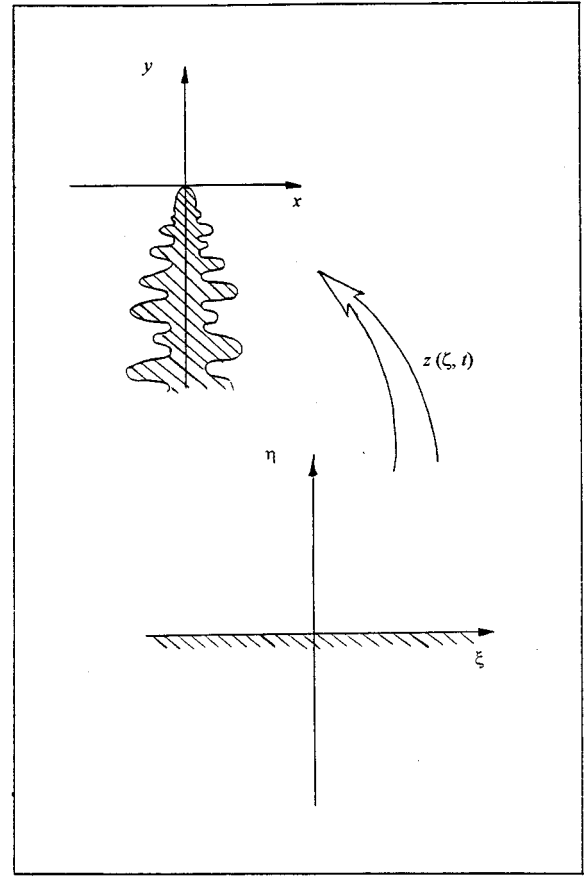

FIG. 2. Conformal map from the computational $\zeta = \xi + i\eta$ plane to the physical $z = x + iy$ plane.

Gibbs-Thomson boundary condition at the interface (see Ref. [38] for a derivation using microscopic physics), which is

$$T = -d_0[1 + \alpha f(\theta)]\kappa \quad \text{on } y = y_i(x,t). \qquad (2.4)$$

Here d_0 is a nondimensional capillary parameter defined by

$$d_0 = \frac{\widetilde{d}_0 c_p}{aL} T_m,$$

where $\widetilde{d}_0$ is the standard capillary length. In Eq. (2.4), κ refers to curvature, while the term $1 + \alpha f(\theta)$ is included to model the anisotropy in the surface energy, where we assume a standard fourfold anisotropy model

$$f(\theta) = 1 - \cos 4(\theta - \theta_0),$$

where θ_0 is the direction of minimal surface energy.

For our purposes, it is convenient to rewrite Eqs. (2.1)–(2.4) in a transformed coordinate system where the interfacial location is known for all times. Consider the conformal transformation $z(\zeta,t)$ that maps the upper-half ζ plane, with $\zeta = \xi + i\eta$ (see Fig. 2) into the exterior of the crystal in the z plane, where $z = x + iy$. It is clear that determination of the function $z(\zeta,t)$ yields the unknown interface $y = y_i(x,t)$, which is always at $\eta = 0$. Under this transformation, the governing equation (2.1) becomes

$$2P|z_\zeta|^2\left[\frac{\partial T}{\partial t}-\text{Re}\left(\frac{z_t}{z_\zeta}\right)\frac{\partial T}{\partial \xi}-\text{Im}\left(\frac{z_t}{z_\zeta}\right)\frac{\partial T}{\partial \eta}\right]$$

$$=2P\left(\text{Im}(z_\zeta)\frac{\partial T}{\partial \xi}+\text{Re}(z_\zeta)\frac{\partial T}{\partial \eta}\right)+\nabla^2 T \quad (2.5)$$

and the far-field condition (2.2) becomes

$$T\to-\Delta \quad \text{as} \quad \eta\to\infty. \quad (2.6)$$

The boundary conditions at the interface correspond to conditions on $\eta=0$, i.e., the real ζ axis

$$T=-d_0[1+\alpha f(\xi,t)]\kappa(\xi,t), \quad (2.7)$$

$$\frac{\partial T}{\partial \eta}=-2P|z_\zeta|^2\,\text{Im}\left(\frac{z_t+i}{z_\zeta}\right), \quad (2.8)$$

where

$$f=1-\frac{1}{|z_\zeta|^4}\,\text{Re}(z_\zeta^4 e^{-i4\theta_0}), \quad (2.9)$$

$$\kappa=-\frac{1}{|z_\zeta|}\,\text{Im}\left(\frac{z_{\zeta\zeta}}{z_\zeta}\right). \quad (2.10)$$

Before considering the asymptotic solution for small P, it is convenient to recover Ivantsov's steady solution with parabolic interface for $d_0=0$ in this notation. Even when $d_0\neq0$ and the dendrite is unsteady, the Ivantsov solution is relevant in matching solutions in the far field, as we shall see momentarily.

The Ivantsov steady solution [6] corresponds to

$$z(\zeta,t)=-i\zeta^2/2+\zeta\equiv z_I(\zeta). \quad (2.11)$$

In this case, T is independent of ξ and is determined from

$$\frac{d^2T}{d\eta^2}+2P(1+\eta)\frac{dT}{d\eta}=0,$$

$$T\to-\Delta \quad \text{as} \quad \eta\to\infty,$$

$$T=0 \quad \text{on} \quad \eta=0. \quad (2.12)$$

It follows that

$$T=T_I(\eta)=-\Delta+\sqrt{\pi P}e^P\text{erfc}[\sqrt{P}(1+\eta)], \quad (2.13)$$

where

$$\Delta=\sqrt{\pi P}e^P\text{erfc}(\sqrt{P}). \quad (2.14)$$

We notice that with the choice $z(\zeta,t)=z_I(\zeta)$ the condition (2.7) on the conservation of heat at the interface reduces to $\partial T/\partial\eta=-2P$, which is satisfied by $T=T_I(\eta)$ at $\eta=0$. We also notice from Eq. (2.13) that for $\eta=O(1)$, the leading-order behavior of the temperature field corresponding to the Ivantsov solution as $P\to0$ is given by

$$T\sim-2P\eta. \quad (2.15)$$

Returning to dimensional variables, the Ivantsov result (2.14) implies that for $d_0=0$, the steady Ivantsov solution

determines only the product of the tip radius a and velocity U in terms of given undercooling and material parameters. This is a well-known degeneracy when surface energy is not taken into account.

A. Asymptotic series in P: Region I equations

In spite of the unwieldy appearance of the governing equations (2.5), simplifications are possible as $\Delta\to0$ (hence $P\to0$). First, we note from Eq. (2.14) that for small undercooling $\Delta=O(P^{1/2})$. Also, we assume that variations occur at most on a dimensional time scale far larger than aP/U, i.e., if $u(\xi,\eta,t)$ is any $O(1)$ quantity of interest, then we assume that

$$P\left|\frac{\partial u}{\partial t}\right|\ll1.$$

This restriction means that the time derivative term in Eq. (2.5) can be neglected to leading order, at least when $|z_\zeta|=O(1)$. We also assume that the interfacial shape approaches the steady Ivantsov shape at sufficiently large distances from the tip. More precisely, if the conformal mapping function is decomposed into

$$z(\zeta,t)=-\frac{i}{2}\zeta^2+\zeta+Z(\zeta,t), \quad (2.16)$$

then we will assume for large but real ζ that

$$|Z|, \quad |Z_t|\ll|\zeta|, \quad |Z_\zeta|\ll1. \quad (2.17)$$

A posteriori checks on general, time-varying solutions are shown to be consistent with the above hypothesis.

The far-field behavior of the Ivantsov temperature field suggests that matching with specified undercooling at infinity will be possible only if we assume $T=O(P)$. Further, consistent with most experimental conditions, we assume $d_0=O(P)$ and note this includes $d_0=o(P)$ as well. Therefore, we define parameter $\mathcal{B}$ through the relation

$$d_0=2\mathcal{B}P, \quad \mathcal{B}=O(1). \quad (2.18)$$

We then form a regular perturbation expansion of the temperature and the conformal mapping function in the form

$$T=PT_0+P^2T_1+O(P^3), \quad (2.19a)$$

$$z=z_0+Pz_1+O(P^2). \quad (2.19b)$$

Then, to $O(P)$, equations and interfacial boundary conditions are

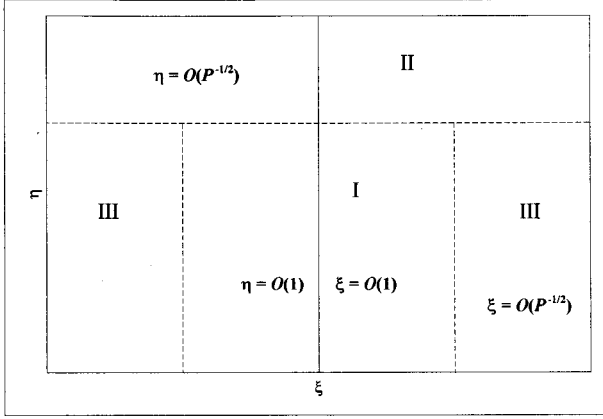$$\nabla^2T_0=0,$$

$$T_0=-2\mathcal{B}(1+\alpha f_0)\kappa_0 \quad \text{on} \quad \eta=0,$$

$$\frac{\partial T_0}{\partial \eta}=-2|z_{0\zeta}|^2\text{Im}\left(\frac{z_{0t}+i}{z_{0\zeta}}\right) \quad \text{on} \quad \eta=0, \quad (2.20)$$

where κ_0 and f_0 refer to the expressions (2.9) and (2.10), with z replaced by z_0.

To next order [i.e., $O(P^2)$] the equations become

FIG. 3. Asymptotic regions in the ζ plane.

$$\nabla^2 T_1 = -2\left(\mathrm{Im}(z_{0\zeta})\,\frac{\partial T_0}{\partial \xi} + \mathrm{Re}(z_{0\zeta})\,\frac{\partial T_0}{\partial \eta}\right) + 2\left(|z_{0\zeta}|^2\,\frac{\partial T_0}{\partial t}\right.$$

$$\left. -\mathrm{Re}[z_{0t}(z_{0\zeta})^*]\,\frac{\partial T_0}{\partial \xi} - \mathrm{Im}[z_{0t}(z_{0\zeta})^*]\,\frac{\partial T_0}{\partial \eta}\right),$$

where

$$T_1 = -2\mathcal{B}[(1+\alpha f_0)\kappa_1 + \alpha f_1 \kappa_0] \quad \text{on} \quad \eta = 0,$$

$$\frac{\partial T_1}{\partial \eta} = -2|z_{0\zeta}|^2\left\{\mathrm{Im}\left(\frac{z_{1t}}{z_{0\zeta}}\right) + \mathrm{Im}\left[\left(\frac{z_{1\zeta}}{z_{0\zeta}}\right)^*\left(\frac{z_{0t}+i}{z_{0\zeta}}\right)\right]\right\}$$

$$\text{on} \quad \eta = 0, \quad (2.21)$$

and

$$\kappa_1 = -\frac{1}{|z_{0\zeta}|}\,\mathrm{Im}\,\frac{d}{d\zeta}\left(\frac{z_{1\zeta}}{z_{0\zeta}}\right) + \frac{1}{|z_{0\zeta}|}\,\mathrm{Re}\left(\frac{z_{1\zeta}}{z_{0\zeta}}\right)\mathrm{Im}\,\frac{z_{0\zeta\zeta}}{z_{0\zeta}},$$

$$f_1 = -\frac{4}{|z_{0\zeta}|^4}\,\mathrm{Re}(z_{0\zeta}^3 z_{1\zeta} e^{-i4\theta_0})$$

$$+ \frac{4}{|z_{0\zeta}|^4}\,\mathrm{Re}[z_{0\zeta}^4 e^{-i4\theta_0}]\mathrm{Re}\,\frac{z_{1\zeta}}{z_{0\zeta}}. \quad (2.22)$$

The set of equations above is not complete since the far-field matching condition as $\eta \to \infty$ is missing. In general, of course, there might be time dependence in the far-field temperature. However, as we shall see later, for certain classes of initial conditions, it is self-consistent to assume that that the far-field temperature is asymptotic to the Ivantsov solution, with its time variation occurring only over a $O(P^{-1})$ scale. For much smaller times, it is appropriate to invoke the Ivantsov solution behavior (2.15) and use that for the leading-order matching to the far field,

$$T_0 \to -2\eta + o(1) \quad \text{as} \quad \eta \to \infty. \quad (2.23)$$

The assumed asymptotic expansion (2.19) is valid for an $O(1)$ region around the tip that is denoted as region I in Fig. 3. Examination of solutions T_1 and z_1, in addition to the leading order T_0 and z_0, will be necessary to define where the assumed expansion (2.19) becomes inconsistent and

hence defines the limits of region I. This question will be investigated later in Secs. II E and II F.

The region I temperature field is obviously harmonic, so a conformal mapping approach is suitable. We notice that the leading-order equation for small Péclet number retains the time derivative in the boundary conditions only. It is significant that this result comes as a consequence of the asymptotic approach rather than from any *ad hoc* hypothesis of a quasisteady approximation.

B. Integro-differential equations for region I

It is convenient to convert the temperature equations in the interior of the domain $\eta > 0$ and the boundary conditions into an equivalent integro-differential equation on a line corresponding to the boundary of the domain, i.e., $\eta = 0$. This further helps analysis of the equations in region I and allows determination of where the assumed asymptotic series expansion in P becomes inconsistent. The resulting integro-differential equation is nearly identical to the equation for the description of interfacial evolution in the displacement of a viscous fluid in a Hele-Shaw cell (see, for instance, [36]), when three-dimensional complications due to thin-film effects are ignored [39]. The only difference here arises in the far field. For the Hele-Shaw flow in the channel geometry, the sidewalls are equivalent to a periodic dependence of shape in a direction perpendicular to the walls. In a radial Hele-Shaw cell, the shape is a closed curve. In both the radial and the channel geometry, the interior of a circle or semicircle is a convenient work plane in the ζ variable. Since we assumed a shape for the dendrite that is asymptotic to an Ivantsov parabola in the far field, it is convenient to use the upper-half ζ plane as the work plane. Further, our previous work on the Hele-Shaw cell has ignored anisotropy in surface energy; here the anisotropy has very important bearing on the dendritic evolution.

The transformation of the mathematical problem involved in the study of the dendrite to one similar to the problem for Hele-Shaw interfacial displacement is a great help since it allows extension of our previous work on the Hele Shaw flows with isotropic surface energy to the dendrite problem in an efficient manner.

Clearly, since T_0 is a harmonic function in two dimensions, we can define the temperature field T_0 as the real part of an analytic function, say, W_0, and decompose it into an Ivantsov contribution and a remaining part. In the same way, we decompose the conformal mapping into the sum of the Ivantsov contribution (which is singular at infinity) and an $O(1)$ perturbation that is analytic in the upper-half plane. Therefore,

$$T_0 = \mathrm{Re}(W_0),$$

$$W_0 = 2i\zeta - 2\mathcal{B}\omega_0(\zeta,t),$$

$$z_0(\zeta,t) = -\frac{i}{2}\,\zeta^2 + \zeta + Z_0(\zeta,t), \quad (2.24)$$

where Z_0 is taken to be analytic everywhere in $\mathrm{Im}\,\zeta > 0$. The Gibbs-Thomson boundary condition (2.20b) becomes

$$\mathrm{Re}(\omega_0) = K_0(\xi,t) \quad \text{on} \quad \eta = 0,$$

where

$$K_0 \equiv [1 + \alpha f_0(\xi,t)] \kappa_0(\xi,t). \quad (2.25)$$

Further, the conservation of heat at the interface (2.20c) takes the form

$$\mathrm{Re}(iW_{0\zeta}) = 2|z_{0\zeta}|^2 \mathrm{Re}\left(i\, \frac{z_{0t}+i}{z_{0\zeta}} \right) \quad \text{on} \quad \eta = 0.$$

With the assumed decomposition of W_0 in Eq. (2.24), it follows that the far-field condition (2.23) is equivalent to

$$\mathrm{Re}(\omega_0) \to 0 \quad \text{as} \quad \zeta \to \infty \quad \text{in} \quad \mathrm{Im}\zeta > 0.$$

The boundary conditions then become a specification of real parts of the complex functions W_0 and ω_0 on the real axis and at infinity. It is well known [40,41] that for a function $F(\zeta)$ that is analytic everywhere in the upper-half plane, including $|\zeta| = \infty$,

$$F(\zeta) = \frac{1}{\pi i} \int_{-\infty}^{+\infty} \frac{d\xi'}{\xi' - \zeta} \mathrm{Re}[F(\xi')] + i\, \mathrm{Im}[F(\infty)],$$

$$\mathrm{Im}\,\zeta > 0. \quad (2.26)$$

Note that $\mathrm{Im}\omega_0(\infty,t) = 0$ without any loss of generality, since this choice does not affect T_0, the quantity of physical interest. Further, from hypothesis (2.17) it follows that $\mathrm{Im}([z_{0t} + i]/z_{0\zeta}) = 0$ at $\zeta = \infty$. Thus, from Eq. (2.25), it follows that for $\mathrm{Im}\,\zeta > 0$,

$$\omega_0(\zeta,t) = \frac{1}{\pi i} \int_{-\infty}^{+\infty} \frac{d\xi'}{\xi' - \zeta} K_0(\xi',t) \equiv I_1(\zeta,t), \quad (2.27)$$

$$\frac{z_{0t}+i}{z_{0\zeta}}(\zeta,t) = \frac{1}{\pi} \int_{-\infty}^{+\infty} \frac{d\xi'}{\xi' - \zeta} R_0(\xi',t) \equiv q_1(\zeta,t), \quad (2.28)$$

where

$$R_0(\zeta,t) = \frac{1 - \mathcal{B}\, \mathrm{Im}\omega_{0\zeta}}{|z_{0\zeta}|^2}. \quad (2.29)$$

Notice that I_1 and q_1 as defined above are analytic in $\mathrm{Im}\zeta > 0$. On approaching the boundary of the domain $\zeta = \xi + i0$, the equations reduce to the integro-differential equations

$$z_{0t} + i = [H_0 + iR_0]z_{0\xi}, \quad (2.30a)$$

$$H_0(\xi,t) = \frac{1}{\pi} \int_{-\infty}^{\infty} \frac{d\xi'}{\xi' - \xi} R_0(\xi',t), \quad (2.30b)$$

$$\mathrm{Im}\omega_{0\xi} = -\frac{1}{\pi} \int_{-\infty}^{\infty} \frac{d\xi'}{\xi' - \xi} \frac{\partial}{\partial\xi'} [K_0(\xi',t)]. \quad (2.30c)$$

We have thus reduced the governing partial differential equation and boundary conditions to a set of integro-differential equations on the real line, whose solution then describes the evolution of z and hence the interfacial motion.

C. Far-field behavior of z_0 and T_0

We need now to ensure that the dynamical equations (2.28) and (2.30c) have solutions that do not violate the *a priori* hypotheses (2.17) and (2.23). The far-field asymptotics of z_0 and T_0, along with those for z_1 and T_1, that are determined here, also help to determine where the assumed asymptotic expansion (2.19) fails.

Clearly Eq. (2.28) can be written as

$$z_{0t} = q_1(\zeta,t)z_{0\zeta} - i. \quad (2.31)$$

Since we assume an initial condition that satisfies the asymptotic requirement

$$z(\zeta,0) \sim -\frac{i}{2}\zeta^2 + \zeta, \quad |\zeta| \to \infty$$

for $t > 0$, we seek a more general time-dependent behavior as $|\zeta| \to \infty$, in the form

$$z_0(\zeta,t) \sim b_2(t)\zeta^2 + b_1(t)\zeta + [b_0(t) - it]. \quad (2.32)$$

Substitution of this expression into Eq. (2.31) and then considering the large-ζ behavior determines the equations for the evolution for $b_j(t)$. That large-ζ analysis requires asymptotic evaluation of q_1 for large $|\zeta|$. To that end, we write q_1 as a sum of three integrals,

$$q_1(\zeta,t) = \frac{1}{\pi} \left(\int_{-\infty}^{-L} + \int_{-L}^{+L} + \int_{+L}^{+\infty} \right) \frac{d\xi'}{\xi' - \zeta} R_0(\xi',t), \quad (2.33)$$

where L is, for convenience, chosen in the range $|\zeta| \gg L \gg 1$. We will then take the limit $L \to \infty$, under the stated ordering relation to $|\zeta|$.

The first and third integrals in Eq. (2.33), referred to as the "outer contribution," combine by introducing the rescaled variable $\xi \equiv |\zeta|\hat{\xi}$. From Eqs. (2.29) and (2.32),

$$z_{0\zeta}(\xi,t) \sim 2b_2(t)|\zeta|\hat{\xi}, \quad R_0(\xi,t) \sim \frac{1}{|4b_2(t)\zeta\hat{\xi}|^2}.$$

So the outer contribution from the integrals in Eq. (2.33) is

$$q_{1,\text{out}} \sim \frac{1}{\pi} \left(\int_{-\infty}^{-L/|\zeta|} + \int_{+L/|\zeta|}^{+\infty} \right) \frac{|\zeta|d\hat{\xi}}{|\zeta|\hat{\xi} - \zeta} \frac{1}{4|b_2(t)|^2|\zeta|^2\hat{\xi}^2}$$

$$= O(|\zeta|^{-1}L^{-1}), \quad (2.34)$$

which vanishes at $L \to \infty$. The $\int_{-L}^{L}$ integral appearing in Eq. (2.33), henceforth the "inner contribution" to q_1, simplifies in the limit $L \to \infty$ to

$$q_{1,\text{in}} \sim -\frac{1}{\pi\zeta} \int_{-L}^{+L} d\xi' R_0(\xi',t) \to -\frac{1}{\pi\zeta} \int_{-\infty}^{+\infty} d\xi' R_0(\xi',t), \quad (2.35)$$

which is $O(\zeta^{-1})$. Since the inner contribution dominates the outer contribution, it follows that to the leading order

$$q_1(\zeta,t) \sim -\frac{1}{\pi\zeta} \int_{-\infty}^{+\infty} d\xi' R_0(\xi',t) \equiv -\frac{M(t)}{\zeta} \quad \text{as } |\zeta| \to \infty.$$
(2.36)

Substituting Eqs. (2.32) and (2.36) into Eq. (2.31), it follows that $\dot{b}_2(t)=0$, therefore from the initial condition $b_2(t)= -i/2$; $\dot{b}_1(t)=0$, therefore $b_1(t)=1$;

$$\dot{b}_0(t) = -2b_2(t)M(t) = \frac{i}{\pi} \int_{-\infty}^{+\infty} d\xi' R_0(\xi',t)$$

$$\text{with } b_0(0)=0. \quad (2.37)$$

Note that $b_0(t)$ is purely imaginary.
  Therefore, as $|\zeta| \to \infty$,

$$z_0(\zeta,t) = -\frac{i}{2}\zeta^2 + \zeta + [b_0(t)-it] + o(1), \quad (2.38)$$

where $b_0(t)$ is determined from Eq. (2.37). This result establishes one hypothesis in Eq. (2.17) that $|Z| \ll |\zeta|$. Further, by differentiating Eq. (2.31) with respect to ζ and t and carrying out a similar analysis for z_{0_ζ} and z_{0_t}, the remainder of the hypotheses in Eq. (2.17) can be established. In the special case where the initial condition is identically the Ivantsov parabola with zero surface energy $\mathcal{B}=0$, $b_0(t) \equiv it$ and z_0 is the Ivantsov solution in the crystal frame, as expected.
  Now we examine the far-field behavior of ω_0. First we note that from the above result, as $\zeta \to \infty$,

$$z_{0\zeta} \sim -i\zeta,$$

while for real ξ tending to $\pm\infty$,

$$f_0(\xi,t) \sim 1 - \cos(4\theta_0) \quad \text{(a constant)},$$

$$\kappa_0(\xi,t) \sim \frac{1}{|\xi|^3},$$

$$K_0(\xi,t) \sim \frac{1+\alpha f_0}{|\xi|^3}. \quad (2.39)$$

In a similar way to what we did for q_1, we write ω_0 as the sum of three integrals

$$\omega_0(\zeta,t) = \frac{1}{\pi i} \left(\int_{-\infty}^{-L} + \int_{-L}^{+L} + \int_{+L}^{+\infty} \right) \frac{d\xi'}{\xi'-\zeta} K_0(\xi',t).$$

Using the asymptotic behavior (2.39), it is easily seen that the contribution from the outer integrals is $O(\zeta^{-1}L^{-2})$. The inner contribution gives us

$$\omega_{0,\text{in}}(\zeta,t) = \frac{1}{\pi i} \int_{-L}^{+L} \frac{d\xi'}{\xi'-\zeta} K_0(\xi',t)$$

$$\sim \frac{-1}{\pi i \zeta} \int_{-\infty}^{+\infty} d\xi' K_0(\xi',t),$$

so that

$$\omega_0(\zeta,t) \sim -\frac{1}{\pi i \zeta} \int_{-\infty}^{+\infty} d\xi' K_0(\xi',t) \quad \text{as } |\zeta| \to \infty. \quad (2.40)$$

Note that we neglected the term involving ω_0 in R_0 in Eq. (2.29), and this result shows that neglect to be consistent. From relation (2.24) it follows that as $\xi^2+\eta^2 \to \infty$,

$$T_0(\xi,\eta,t) \sim -2\eta - \frac{2\mathcal{B}\eta}{\pi(\xi^2+\eta^2)} \int_{-\infty}^{+\infty} d\xi' K_0(\xi',t). \quad (2.41)$$

D. Far-field behavior of z_1 and T_1

  We now turn to the far-field solutions for the z_1 and T_1. From Eqs. (2.38) and (2.39), it follows that as $\zeta \to \infty$,

$$\nabla^2 T_1 \sim -4i\dot{b}_0(t)(1+\eta) - \frac{4\mathcal{B}\eta}{\pi}\left(1+\frac{2\eta}{\xi^2+\eta^2}\right)$$

$$\times \int_{-\infty}^{+\infty} d\xi' \frac{\partial K_0}{\partial t}(\xi',t) + o(1). \quad (2.42)$$

We decompose T_1 into

$$T_1 = T_{1H} + T_{1P}, \quad (2.43)$$

where T_{1P} is a particular solution to the inhomogeneous differential equation in Eq. (2.42) and T_{1H} is harmonic. It is convenient to choose the particular solution so that, as $\zeta \to \infty$,

$$T_{1P}(\xi,\eta,t) \sim -2i\dot{b}_0(t)\left(1+\frac{1}{3}\eta\right)\eta^2$$

$$-\frac{2\mathcal{B}}{3\pi}\eta^3 \int_{-\infty}^{+\infty} d\xi' \frac{\partial K_0}{\partial t}(\xi',t)$$

$$+\frac{2\mathcal{B}\xi\eta}{\pi}\tan^{-1}\left(\frac{\eta}{\xi}\right)\int_{-\infty}^{+\infty} d\xi' \frac{\partial K_0}{\partial t}(\xi',t).$$

Notice that while the above expression is only asymptotic, $T_{1P}(\xi,0,t)$ cannot grow with $|\xi|$ since in that case such a term would have been present in this expression. From the boundary condition for T_1, we require of T_{1H} that

$$T_{1H}(\xi,0,t) = -2\mathcal{B}K_1(\xi,t) - T_{1P}(\xi,0,t),$$

$$K_1 = (1+\alpha f_0)\kappa_1 + \alpha f_1 \kappa_0.$$

Since $K_1(\xi,t)$, the curvature correction, vanishes for large ξ while $T_{1P}(\xi,0,t)$ tends to zero, it follows from Poisson's integral formula that

$$T_{1H}(\xi,\eta,t) = \frac{1}{\pi}\int_{-\infty}^{\infty} d\xi' \frac{\eta}{\eta^2+(\xi-\xi')^2}$$

$$\times [-2\mathcal{B}K_1(\xi,t) - T_{1P}(\xi,0,t)]. \quad (2.44)$$

Therefore, as $\xi^2+\eta^2 \to \infty$,

$$T_1 \sim -2i\dot{b}_0(t)\left(1+\frac{1}{3}\,\eta\right)\eta^2 - \frac{2\mathcal{B}}{3\pi}\,\eta^3 \int_{-\infty}^{+\infty} d\xi' \frac{\partial K_0}{\partial t}(\xi',t)$$

$$+ O(\mathcal{B}\eta^2). \qquad (2.45)$$

Next we implement the boundary condition on $\partial T_1/\partial\eta$ in order to determine the large-$|\zeta|$ evolution of z_1. We find from Eq. (2.21) the condition

$$\frac{\partial T_1}{\partial\eta} = 2|z_{0\zeta}|^2 \operatorname{Re}\left[i\,\frac{z_{1t}}{z_{0\zeta}} - i\left(\frac{z_{1\zeta}}{z_{0\zeta}}\right)\left(\frac{z_{0t}+i}{z_{0\zeta}}\right)^*\right]. \qquad (2.46)$$

For $\operatorname{Im}\zeta>0$, $(z_0+i)/z_{0\zeta} = q_1(\zeta,t)$, as defined in Eq. (2.28). Its analytic continuation to the real axis is H_0+iR_0, as given in Eq. (2.30), and since the asymptotic relation (2.36) holds on the real axis as well, it follows that

$$\left(\frac{z_{0t}+i}{z_{0\zeta}}\right)^* \sim M(t)/\zeta \quad \text{as } |\zeta|\to\infty \quad \text{on } \operatorname{Im}\zeta=0. \qquad (2.47)$$

Further simplification of Eq. (2.46) is possible by making an *a priori* hypothesis, which may be relaxed subsequently, that $z_{1\zeta}$ does not grow any faster than $|\zeta|$ as $\zeta\to\pm\infty$. Then Eq. (2.46) becomes

$$\operatorname{Re}\left[i\,\frac{z_{1t}}{z_{0\zeta}} - iM(t)\left(\frac{z_{1\zeta}}{(\zeta+i)z_{0\zeta}}\right)\right] \equiv R_1(\zeta,t), \qquad (2.48)$$

where

$$R_1(\xi,t) = \frac{1}{2|z_{0\zeta}(\xi,t)|^2}\frac{\partial T_1}{\partial\eta}(\xi,0,t) + \operatorname{Re}\left[+i\left(\frac{z_{1\zeta}(\xi,t)}{z_{0\zeta}(\xi,t)}\right)\right.$$

$$\left.\times[q_1^*(\xi,t) - M(t)/(\xi+i)]\right]. \qquad (2.49)$$

From the asymptotic behavior $z_{0\zeta}\sim -i\zeta$, $T_1\sim\xi^2+\eta^2$, and the assumed restriction on the growth rate of z_1, it follows that $R_1(\xi,t)\to0$ as $\xi\to\pm\infty$. Since the quantity enclosed in square brackets on the left-hand side of Eq. (2.48) is obviously analytic in the upper-half ζ plane, application of the Cauchy half-plane formula once again gives

$$z_{1t} - \frac{M(t)}{\zeta+i}\,z_{1\zeta} = \left\{-\frac{z_{0\zeta}}{\pi}\int_{-\infty}^{+\infty}\frac{d\xi'}{\xi'-\zeta}R_1(\xi',0,t)\right\}$$

$$\text{in } \operatorname{Im}\zeta>0. \qquad (2.50)$$

Since the right-hand side of Eq. (2.50) can at most be asymptotic to a constant for large $|\zeta|$, it follows that z_{1t} $\sim$ (spatial constant) as $|\zeta|\to\infty$. [Notice that the second term in Eq. (2.50) is higher order.] Therefore, because z_1 is initially zero, its solution at large $|\zeta|$ must take the form

$$z_1 \sim A(t),$$

$$\dot{A}(t) = \frac{1}{2\pi i}\int_{-\infty}^{+\infty} d\xi' R_1(\xi',0,t),$$

$$A(0) = 0. \qquad (2.51)$$

The *a priori* hypothesis on the magnitude of z_1 that we used above can now be relaxed by seeking higher-order corrections the asymptotic behavior of q_1 and subtracting appropriate analytic terms [instead of just $M/(\zeta+i)$] in the form $M(t)/(\zeta+i) + M_1(t)/(\zeta+i)^2 + \cdots$ up to terms of sufficiently high order, from both the left- and right-hand sides of Eq. (2.48). This procedure ensures that R_1 still goes to zero at $\pm\infty$ any time z_1 does not grow any faster than some polynomial. In a more general case we conclude that Eq. (2.51) represents the asymptotic behavior of z_1 for large $|\zeta|$. Therefore, the two-term asymptotic expansion for z in (small) Péclet number (2.19b) is uniformly valid as $|\zeta|\to\infty$.

E. Far-field breakdown of region I equations: Region II

The asymptotic solutions derived above indicate that the regular perturbation breaks down once we are sufficiently far from the crystal tip, in a fashion to be discovered in this section. While the conformal mapping has the far-field behavior (in the crystal frame)

$$z \sim -\frac{i}{2}\,\zeta^2 + \zeta + [b_0(t) - it] + PA(t) \qquad (2.52)$$

and remains a regular perturbation expansion as $\operatorname{Im}\zeta\to\infty$, the two-term asymptotic expansion of the temperature field worked out previously,

$$T \sim -2P\eta + P^2\,\frac{\eta^3}{3}\left[2i\dot{b}_0(t) - 2\mathcal{B}\int_{-\infty}^{+\infty} d\xi'\frac{\partial K_0}{\partial t}(\xi',t)\right]$$

$$\text{as } |\zeta|\to\infty, \qquad (2.53)$$

clearly suggests that the asymptotic series (2.19) fails when $\eta = O(P^{-1/2})$. Therefore, we are forced to define a new asymptotic region, say region II (see Fig. 3), where the appropriate scaling of dependent and independent variables takes the form

$$T \sim P^{1/2}T_0 + O(P^{3/2}), \quad \zeta+i = P^{-1/2}\zeta', \quad t = P^{-1}\tau. \qquad (2.54)$$

The equations for the evolution of T in region II are then determined by taking $P\to0$ with ζ' fixed in Eq. (2.5). The first term in the asymptotic series in region II satisfies the equation

$$2[(\xi')^2 + (\eta')^2]\frac{\partial T_0}{\partial\tau} = (\nabla')^2 T + 2\left(-\xi'\frac{\partial T_0}{\partial\xi'} + \eta'\frac{\partial T_0}{\partial\eta'}\right),$$

$$T_0 \to -\sqrt{\pi} \quad \text{as } \eta'\to\infty, \qquad (2.55)$$

and in order to match to region I, we require that

$$T_0 \sim -2\eta' \quad \text{as } \eta'\to0,$$

i.e., T_0 matches the solution in region I. In deriving Eq. (2.55) we used the fact that the conformal mapping function z in region II is still given by the Ivantsov solution $-i\zeta^2/2 + \zeta$, at least to the leading order. Thus there is no need to write an equation for the mapping function.

The evolution in region II occurs on a slow $O(P^{-1})$ intrinsic time scale. In general, time dependence can come in through the matching to other regions (for instance, to region I). However, for $t = O(1)$, with the matching condition and condition at infinity being independent of t, it follows that the initial Ivantsov solution is the appropriate leading-order solution in region II and therefore

$$T_0 = -\sqrt{\pi}\ \mathrm{erf}(\eta'). \qquad (2.56)$$

F. Equations in region III

The existence of region II is inferred from the breakdown of the asymptotic expansion for large η; however, differing scalings can be expected when $\eta = O(1)$, but $|\xi|$ is large. Clearly the governing equation in region I cannot be valid when $|z_{0_\zeta}|^2 = O(P^{-1})$, as seen directly from Eq. (2.5).

Standard arguments give the appropriate scaling in this (new) region III as $\xi = P^{-1/2}\xi'$ and the asymptotic expansion for the temperature field is here given by

$$T = PT_0 + O(P^2), \qquad (2.57)$$

where T_0 satisfies

$$2(\xi')^2 \frac{\partial T_0}{\partial t} = \frac{\partial^2 T_0}{\partial \eta^2}, \qquad (2.58)$$

with boundary conditions

$$T_0 = 0 \quad \text{on} \ \eta = 0,$$

$$\frac{\partial T_0}{\partial \eta} = -2 \quad \text{on} \ \eta = 0. \qquad (2.59)$$

Matching to region II requires that

$$T_0 \sim -2\eta \quad \text{for} \ \eta \to \infty. \qquad (2.60)$$

Notice that this problem, with conditions on both T_0 and $\partial T_0/\partial \eta$ on $\eta = 0$ as well as the matching condition at $\eta = \infty$, is overspecified. However, from our previous work, we know that in this region the asymptotic behavior of z is $z \sim -i\zeta^2/2 + \zeta$, so that the free boundary is known *a priori*. Indeed, the steady solution (corresponding to Ivantsov solution)

$$T_0 = -2\eta \qquad (2.61)$$

satisfies Eq. (2.58) and all the boundary and matching conditions (2.59) and (2.60). This steady solution is indeed correct for region III until disturbances originating in region I have had time to advect into this region. As we shall see in the further analysis of the region I equations, this time is at least $O(P^{-1})$. When disturbances from region I do finally arrive, the equations must be modified to reflect the fact that z is no longer given by the Ivantsov solution; the additional

boundary condition then determines the dynamics of the free surface, as well as the temperature distribution.

We conclude by noting that regions II and III play no active role in the dynamics of region I, which is fortuitous since it allows us to conclude a great deal about dendritic behavior based solely on region I dynamics, for rather long times. From now on, in this paper we concentrate solely on dynamics implied by the region I equations.

We begin the process of studying the region I dynamics in the next section by investigating the linear theory for growth of localized disturbances, a problem directly related to earlier work by Caroli, Caroli, and Roulet [18] and Barber, Barbieri, and Langer [16]. Since all of what follows involves investigation of solutions for the first term in the Péclet number series (2.19), we now drop, for simplicity, the $(\ )_0$ notation in reference to that first term, i.e., from this point forward, $z(\zeta, t)$ refers to the conformal mapping in region I, to leading order in P.

III. LINEAR THEORY FOR GROWTH OF LOCALIZED DISTURBANCES IN REGION I

We consider here the fate of small localized shape disturbances initially located near the tip (in region I) in the form of one or more narrow perturbations superposed on a steady or unsteady dendrite solution, using a linearized analysis. With a Green's-function approach, a similar analysis relying on wave-packet hypotheses has been carried out by Caroli, Caroli, and Roulet [18] and Barber, Barbieri, and Langer [16] the results from each indicating a different rate of growth for the disturbances; the results of Barber, Barbieri, and Langer [16] are consistent with the numerical results of Kessler and Levine [17]. Our study differs from previous approaches in that we derive very general results for the evolution of a short-wavelength disturbance superposed on an arbitrary time-evolving base state. Since we do not assume the background state to be steady, the growth rate may be calculated for any given unsteady solution, provided that the background state does not have spatial scales of the same order as or smaller than that of the superposed localized disturbance. Further, our approach, using a Fourier transform, does not make any *a priori* wave-packet ansatz. For the case of a steady background state, concrete results can be obtained for the growth rate as a function of (large) distance from the tip (though still within region I). We obtain below a solution that is consistent with that of Barber, Barbieri, and Langer [16].

The linearized problem is approached below in two complementary ways. In Sec. III A we study the equations in the real ζ domain and obtain results through a Fourier-transform method. In Sec. III B we study the dynamics of the analytically continued equations in the lower-half complex ζ plane. Aside from confirming the results in Sec. III A, we demonstrate how noise amplification and wave-packet evolution are in fact connected to the motion toward the real axis of complex singularities of the idealized zero-surface energy problem.

We begin the linear analysis by decomposing the conformal mapping function z in region I into

$$z = z^0 + z^1, \qquad (3.1)$$

where z^0 corresponds to the given solution, steady or unsteady, and z^1 corresponds to the disturbance with small-scale spatial variations. We will also assume here that $|z_\xi^1| \ll |z_\xi^0|$ and $|z_{\xi\xi}^1| \ll |z_{\xi\xi}^0|$. Then z^1, to the leading order, satisfies the linear equation

$$z_t^1 = [H^0 + iR^0]z_\xi^1 + [H^1 + iR^1]z_\xi^0, \qquad (3.2)$$

where

$$R^0(\xi,t) = \frac{1 - \mathcal{B} \, \mathrm{Im}\omega_\xi^0}{|z_\xi^0|^2}, \qquad (3.3)$$

$$H^0(\xi,t) = \frac{1}{\pi} \fint_{-\infty}^{\infty} \frac{d\xi'}{\xi' - \xi} R^0(\xi',t), \qquad (3.4)$$

$$\mathrm{Im}\omega_\xi^0 = -\frac{1}{\pi} \fint_{-\infty}^{\infty} \frac{d\xi'}{\xi' - \xi} \frac{\partial}{\partial \xi'} K_0(\xi',t), \qquad (3.5)$$

$$K_0(\xi,t) = -[1 + \alpha f_0(\xi,t)]\left[\frac{1}{|z_\xi^0|} \, \mathrm{Im}\left(\frac{z_{\xi\xi}^0}{z_\xi^0}\right)\right], \qquad (3.6)$$

$$f_0(\xi,t) = 1 - \mathrm{Re}\left(\frac{z_\xi^{0^4} e^{-i4\theta_0}}{|z_\xi^0|^4}\right), \qquad (3.7)$$

$$R^1(\xi,t) = -2\frac{1 - \mathcal{B} \, \mathrm{Im}\omega_\xi^0}{|z_\xi^0|^2} \, \mathrm{Re}\left[\frac{z_\xi^1}{z_\xi^0}\right] - \frac{\mathcal{B} \, \mathrm{Im}\omega_\xi^1}{|z_\xi^0|^2}, \qquad (3.8)$$

$$H^1(\xi,t) = \frac{1}{\pi} \fint_{-\infty}^{\infty} \frac{d\xi'}{\xi' - \xi} R^1(\xi',t), \qquad (3.9)$$

$$\mathrm{Im}\omega_\xi^1(\xi,t) = -\frac{1}{\pi} \fint_{-\infty}^{\infty} \frac{d\xi'}{\xi' - \xi} \frac{\partial}{\partial \xi'} K_1(\xi',t), \quad (3.10)$$

$$K_1(\xi,t) = -[1 + \alpha f_0(\xi,t)]\left[-\frac{1}{|z_\xi^0|} \, \mathrm{Im}\left(\frac{z_{\xi\xi}^0}{z_\xi^0}\right)\mathrm{Re}\left(\frac{z_\xi^1}{z_\xi^0}\right)\right.$$
$$\left. + \frac{1}{|z_\xi^0|} \, \mathrm{Im}\frac{\partial}{\partial \xi}\left(\frac{z_\xi^1}{z_\xi^0}\right)\right] - \frac{\alpha f_1(\xi,t)}{|z_\xi^0|} \, \mathrm{Im}\left(\frac{z_{\xi\xi}^0}{z_\xi^0}\right), \quad (3.11)$$

$$f_1(\xi,t) = \frac{4}{|z_\xi^0|^4} \, \mathrm{Re}[(z_\xi^0)^3 e^{-i4\theta_0}]$$
$$- \frac{\mathrm{Re}[4(z_\xi^0)^4 e^{-i4\theta_0}]}{|z_\xi^0|^4} \, \mathrm{Re}\left[\frac{z_\xi^1}{z_\xi^0}\right]. \qquad (3.12)$$

The integrals in the above expressions must be interpreted as Cauchy principal value integrals and therefore each is displayed as an integral with a horizontal dash.

In what follows we will suppose that the disturbance z^1 is characterized by very short scales, which may arise from, but are not limited to, isolated narrow structures. Formally, then, we take the functional dependence of z^1 on ξ to be through ξ/ϵ, $\epsilon \ll 1$, where ϵ is then a measure of the spatial scale of the disturbance. Hence we write $z^1(\xi,t) = Z(\xi/\epsilon,t)$ for some function Z. The base state z^0 and its derivatives are assumed to be independent of ϵ. Such a hypothesis for z^1 allows great simplification of the equations given above. It is clear from

Eqs. (3.10) and (3.11) that for $\epsilon \ll 1$, the third-derivative term provides the dominant contribution to the integrand in Eq. (3.10). Further, it is well known that for smooth functions $S(\xi)$ and $T(\xi/\epsilon)$, for which the Hilbert transforms exist,

$$\frac{1}{\pi} \fint_{-\infty}^{\infty} \frac{d\xi'}{\xi' - \xi} T\left(\frac{\xi'}{\epsilon}\right) S(\xi')$$
$$\sim \frac{S(\xi)}{\pi} \fint_{-\infty}^{\infty} \frac{d\xi'}{\xi' - \xi} T\left(\frac{\xi'}{\epsilon}\right) \quad \text{for} \ \epsilon \to 0. \qquad (3.13)$$

Further, since $z_{\zeta\zeta\zeta}^1/z_\zeta^0$ is an analytic function in the upper-half ζ plane and goes to zero at ∞ sufficiently rapidly, it follows that

$$\frac{1}{\pi} \fint_{-\infty}^{\infty} \frac{d\xi'}{\xi' - \xi} \, \mathrm{Im}\left(\frac{z_{\xi\xi\xi}^1(\xi',t)}{z_\xi^0(\xi',t)}\right) = \mathrm{Re}\left(\frac{z_{\xi\xi\xi}^1(\xi,t)}{z_\xi^0(\xi,t)}\right). \quad (3.14)$$

Therefore, from Eqs. (3.10)–(3.12),

$$\mathrm{Im}\omega_\xi^1 \sim \frac{1 + \alpha f_0(\xi,t)}{|z_\xi^0|} \, \mathrm{Re}\left[\frac{z_{\xi\xi\xi}^1}{z_\xi^0}\right]. \qquad (3.15)$$

Further, we note that R^1 in Eq. (3.8) contains two terms: The first term is $O(\epsilon^{-1})$, while the second term, on using Eq. (3.15), is $O(\mathcal{B}\epsilon^{-3})$. We retain both terms since $\mathcal{B}$ may be small. In evaluating H^1 through the Hilbert transform integral, we invoke the property (3.13) above and obtain an expression for H^1 that is asymptotically correct for $\epsilon \to 0$. Combining this expression for H^1 with the leading-order behavior of R^1 in Eq. (3.8), we obtain

$$[H^1 + iR^1]z_\xi^0 \sim -2i\left\{\frac{1 - \mathcal{B} \, \mathrm{Im}\omega_\xi^0}{|z_\xi^0|^2}\right\}z_\xi^1$$
$$- \frac{i\mathcal{B}[1 + \alpha f_0(\xi,t)]}{|z_\xi^0|^3} z_{\xi\xi\xi}^1. \qquad (3.16)$$

Notice that the coefficient of z_ξ^1 in the above is just $-2iR^0$. So combining with $(H^0 + iR^0)z_{0_\xi}$ appearing in Eq. (3.2), we obtain the following simplification of Eq. (3.1), valid in the asymptotic limit $\epsilon \to 0$:

$$z_t^1 = [H^0 - iR^0]z_\xi^1 - \frac{i\mathcal{B}[1 + \alpha f_0(\xi,t)]}{|z_\xi^0|^3} z_{\xi\xi\xi}^1. \qquad (3.17)$$

Equation (3.17) forms the basis for further analysis presented in Secs. III A and III B.

A. Growth of a disturbance—Fourier-transform approach

We now specialize Eq. (3.17) to the case for which there is a confined, small-scale initial disturbance. Since that disturbance will be advected along the crystal surface, it is convenient to introduce a variable

$$\chi \equiv [\xi - \xi_d(t)]/\epsilon, \qquad (3.18)$$

where $\xi_d(t)$ is evolved according to

$$\dot{\xi}_d(t) = -H^0(\xi_d(t),t). \qquad (3.19)$$

We define $Z^1(\chi,t)$ through the relation

$$z^1(\xi_d(t)+\epsilon\chi,t)=Z^1(\chi,t). \qquad (3.20)$$

Then, to the leading order, Eq. (3.17) becomes

$$Z_t^1 \sim -i\epsilon^{-1}R^0(\xi_d(t),t)Z_\chi^1 - \frac{i\mathcal{B}\epsilon^{-3}[1+\alpha f_0(\xi_d(t),t)]}{|z_\xi^0(\xi_d(t),t)|^3}Z_{\chi\chi\chi}^1. \qquad (3.21)$$

This equation is adequate for studying the evolution of Z^1 over an $O(\epsilon)$ time scale: however, it is not accurate over an $O(1)$ time scale since we ignored $O(1)$ terms in approximating Eq. (3.17) by Eq. (3.21). Including these corrections, Eq. (3.21) is replaced by

$$Z_t^1 = [-i\epsilon^{-1}R^0(\xi_d(t),t)+H_\xi^0(\xi_d(t),t)\chi - iR_\xi^0(\xi_d(t),t)\chi]Z_\chi^1$$
$$- \frac{i\mathcal{B}\epsilon^{-3}}{|z_\xi^0(\xi_d(t),t)|^3}Z_{\chi\chi\chi}^1. \qquad (3.22)$$

We now introduce the Fourier transform of Z^1,

$$Z^1(\chi,t)=\int_0^\infty dk\; e^{ik\chi}\hat{Z}^1(k,t), \qquad (3.23)$$

where the integration range reflects the fact that $Z^1(\chi,t)$ is analytic in the upper-half plane. It follows that

$$\hat{Z}^1(k,t)=\frac{1}{2\pi}\int_{-\infty}^\infty d\chi\; e^{-ik\chi}Z^1(\chi,t). \qquad (3.24)$$

If we now introduce for convenience $Q=k\hat{Z}^1(k,t)$, then it follows from Eq. (3.22) that

$$Q_t + k(H_\xi^0(\xi_d,t)-iR_\xi^0(\xi_d,t))Q_k$$
$$= \frac{1}{\epsilon}\left[kR^0(\xi_d,t)-\frac{\mathcal{B}[1+\alpha f_0(\xi_d,t)]k^3}{\epsilon^2|z_\xi^0|^3}\right]Q. \qquad (3.25)$$

Using the characteristic direction in k-t space,

$$\lambda = k\,\exp\left[-\int_0^t dt'[H_\xi^0(\xi_d(t'),t')=-iR_\xi^0(\xi_d(t'),t')]\right], \qquad (3.26)$$

it is possible to integrate Eq. (3.25) along the λ characteristic, in terms of an initial value $\hat{Z}^1(k,0)$. The result may then be put in the final form

$$\hat{Z}^1(k,t)=\hat{Z}^1(k,0)\exp\left[\frac{k}{\epsilon}\Sigma_1(t)-\frac{\mathcal{B}k^3}{\epsilon^3}\Sigma_2(t)\right], \qquad (3.27)$$

where

$$\Sigma_1(t)=\int_0^t\exp\left\{\int_0^{t'}[H_\xi^0(\xi_d(\tilde{t}),\tilde{t})-iR_\xi^0(\xi_d(\tilde{t}),\tilde{t})]d\tilde{t}\right\}$$
$$\times R^0(\xi_d(t'),t')dt'\,\exp\left\{-\int_0^t[H_\xi^0(\xi_d(t'),t')\right.$$
$$\left.-iR_\xi^0(\xi_d(t'),t')]dt'\right\}, \qquad (3.28)$$

$$\Sigma_2(t)=\int_0^t\left[\frac{1+\alpha f_0(\xi_d(t'),t')}{|z_\xi^0(\xi_d(t'),t')|^3}\right]$$
$$\times\int_0^{t'}\exp\left\{3\int_0^{t'}[H_\xi^0(\xi_d(\tilde{t}),\tilde{t})-iR_\xi^0(\xi_d(\tilde{t}),\tilde{t})]d\tilde{t}\right\}$$
$$\times\exp\left\{-3\int_0^t[H_\xi^0(\xi_d(t'),t')-iR_\xi^0(\xi_d(t'),t')]dt'\right\}. \qquad (3.29)$$

Thus

$$\hat{Z}^1(\chi,t)=\int_0^\infty dk\;\hat{Z}^1(k,0)\exp\left[ik\chi+\frac{k}{\epsilon}\Sigma_1(t)-\frac{\mathcal{B}k^3}{\epsilon^3}\Sigma_2(t)\right]. \qquad (3.30)$$

If either t is sufficiently large or $\mathcal{B}$ sufficiently small, then $\Sigma_2\ll1$ and therefore $(i\chi\epsilon+\Sigma_1)^{3/2}\gg\sqrt{\mathcal{B}\Sigma_2}$. Then this integral may be asymptotically evaluated by steepest descent; we obtain

$$Z^1(\chi,t)\sim\epsilon\hat{Z}^1(\epsilon k_0,0)\left(\frac{\pi^2}{3\mathcal{B}\Sigma_2(i\epsilon\chi+\Sigma_1)}\right)^{1/4}$$
$$\times\exp\left[\frac{2}{3\sqrt{3\mathcal{B}\Sigma_2}}(i\epsilon\chi+\Sigma_1)^{3/2}\right], \qquad (3.31)$$

where the saddle point is located at $k_{\mathrm{SP}}=\epsilon k_0$ for

$$k_0=\left(\frac{i\epsilon\chi+\Sigma_1}{3\mathcal{B}\Sigma_2}\right)^{1/2}. \qquad (3.32)$$

The result (3.31) is valid for any background state z^0, steady or unsteady, where Σ_1, Σ_2, and k_0 are computed from Eqs. (3.28), (3.29), and (3.32) once R^0, H^0, and their derivatives with respect to ξ are computed using the given $z^0(\xi,t)$ in Eqs. (3.3)–(3.7), while $\xi_d(t)$ is found by solving Eq. (3.19).

More concrete expressions for the growth rate can be obtained with more specific knowledge of $z^0(\xi,t)$. For instance, the trajectory equation (3.19) for $\xi_d(t)$ can be solved explicitly when $z^0(\xi,t)=\xi-(i/2)\xi^2$, corresponding to the Ivantsov solution. The corresponding $H^0(\xi,t)$ is simply $-\xi/(\xi^2+1)$. On integrating Eq. (3.19) we obtain

$$\xi_d^2+2\ln|\xi_d|=\mathrm{const}+2t. \qquad (3.33)$$

It follows from the above that if $\xi_d(0)>0$, then $\xi_d(t)$ increases monotonically and asymptotically behaves as $\sqrt{2t}$ for $t\gg1$. For steady base states close to the Ivantsov solution, which is appropriate for small α [12], Eq. (3.33) gives a good approximation to the actual trajectory of $\xi_s(t)$, which will be discussed in Sec. III B.

More generally, if the base state is not close to the Ivantsov except in the far field or if the interface is not steady, we can still simplify the expression (3.31) for $t\gg1$, provided we assume that $|\xi_d(t)|$, which is initially $O(1)$, is at some point sufficiently large. In that case, from Eqs. (3.4)

and (3.19), it follows that if $|z_\xi^0|^2$ is $O(\xi^2)$ and $\mathcal{B}\,\mathrm{Im}\,\omega_\zeta^0 = O(1)$ for $|\xi| \gg 1$, then $H^0(\xi,t) \sim -M/\xi$ and therefore as $t \to \infty$,

$$\xi_d(t) \sim \sqrt{\int_0^t 2M\,dt} \quad \text{where} \quad M = \frac{1}{\pi}\int_{-\infty}^{\infty} d\xi\,R^0(\xi,t)$$
(3.34)

for positive ξ_d. If it turns out that $\xi_d(0) < 0$, then repeating the above arguments gives, for $t \to \infty$,

$$\xi_d(t) \sim -\sqrt{\int_0^t 2M\,dt}.$$
(3.35)

From this point onward we examine only positive $\xi_d(t)$, from obvious symmetry considerations. The expressions (3.28) and (3.29) for Σ_1 and Σ_2 simplify as well for $t \gg 1$ and $\xi_d(t) \gg 1$ and take the much simpler form

$$\Sigma_1 \sim \frac{1}{\xi_d(t)}\int^t R^0(\xi_d(t'),t')\xi_d(t')dt',$$
(3.36)

$$\Sigma_2(t) \sim \frac{1}{\xi_d^3}\int^t dt'\,\frac{\xi_d^3(t')}{|z_\xi^0(\xi_d(t'),t')|^3}\,[1+\alpha f_0(\xi_d(t'),t')].$$
(3.37)

If we now suppose that the disturbance has traveled sufficiently far from its initial location so that $\xi_d(t)$ is large enough to make the base state well approximated by the Ivantsov form $z_\xi^0(\xi_d,t) \sim -i\xi_d$, then

$$R^0(\xi_d(t),t) \sim \frac{1}{\xi_d^2(t)},$$

$$f_0(\xi_d(t),t) \sim 1 - \cos(4\theta_0) \equiv f_0^0 \quad \text{(a constant)} \quad \text{for } t \to \infty.$$
(3.38)

(This result is not valid if the base state has time dependence that has propagated to ξ_d or further.) If $\theta_0 = 0$, so that the minimal surface energy direction coincides with the η axis, i.e., the y axis, then $1 + \alpha f_0^0 \sim 1$ even when α is not small; the anisotropy therefore plays no role in the asymptotic growth rate of the disturbance according to linear theory. While it is straightforward to include the case $\theta_0 \neq 0$ in the calculations, we will henceforth limit our discussions to $\theta_0 \equiv 0$. Under the simplifications of Eq. (3.38), then Σ_1 and Σ_2, given in Eqs. (3.36) and (3.37), further simplify to

$$\Sigma_1 \sim \frac{1}{\xi_d(t)}\int^t \frac{1}{\xi_d(t')}\,dt'$$
(3.39)

$$\Sigma_2(t) \sim \frac{t}{\xi_d^3}$$
(3.40)

and the large-t asymptotic form (3.31) becomes

$$Z^1(\chi,t) \sim \epsilon\hat{Z}^1(\epsilon k_0,0)\left(\frac{\pi^2\xi_d^3}{3\mathcal{B}t(i\epsilon\chi+\Sigma_1)}\right)^{1/4}$$
$$\times\exp\left[\frac{2\sqrt{\xi_d^3}}{3\sqrt{3}\mathcal{B}}(i\epsilon\chi+\Sigma_1)^{3/2}\right].$$
(3.41)

An additional assumption on the base state z^0 that makes M approach a constant value for $t \to \infty$ implies

$$\xi_d(t) \sim \sqrt{2Mt}, \quad \Sigma_2 \sim \frac{1}{2M\xi_d},$$

$$\Sigma_1 \sim \frac{1}{M},$$

$$k_0 \sim \sqrt{\frac{2M\xi_d(t)(1+i\epsilon M\chi)}{3\mathcal{B}}}$$

and therefore

$$Z^1(\chi,t) \sim \epsilon\hat{Z}^1(\epsilon k_0,0)\left(\frac{2\pi^2 M^2\xi_d}{3\mathcal{B}(iM\epsilon\chi+1)}\right)^{1/4}$$
$$\times\exp\left[\frac{2^{3/2}\xi_d^{1/2}}{3^{3/2}M\mathcal{B}^{1/2}}(1+iM\epsilon\chi)^{3/2}\right].$$
(3.42)

Though the result (3.42) holds for $M \to \text{const}$ for $t \to \infty$, z^0 need not necessarily be steady for this to be so.

Specializing still further to the situation for which z^0 is a steady state that is close to the Ivantsov solution $z^0 = -(i/2)\zeta^2 + \zeta$, which is valid for small, nonzero α, it is appropriate to substitute $M = 1$ in Eq. (3.42). In that case, the result is consistent with that of Barber, Barbieri, and Langer [16], though without the algebraic prefactor $(1+iM\chi\epsilon)^{-1/4}$. We also note from Eq. (3.42) that the dependence on the precise form of initial condition is weak. For instance, if

$$Z^1(\xi,0) = \frac{\delta}{\xi - \xi_s(0) - i\eta_s(0)},$$
(3.43)

then

$$\epsilon\hat{Z}^1(\epsilon k_0,0) = -i\delta e^{k_0\eta_s(0)}.$$
(3.44)

So, in that case

$$Z^1(\chi,t) \sim -i\delta\exp\left[\eta_s(0)\left(\frac{2M\xi_d(iM\epsilon\chi+1)}{3\mathcal{B}}\right)^{1/2}\right]$$
$$\times\left(\frac{2\pi^2 M^2\xi_d}{3\mathcal{B}(iM\epsilon\chi+1)}\right)^{1/4}$$
$$\times\exp\left[\frac{2\sqrt{2\xi_d}}{3M\sqrt{3\mathcal{B}}}(iM\epsilon\chi+1)^{3/2}\right].$$
(3.45)

Since $|\eta_s(0)| = O(\epsilon)$, which is essential for an initially localized disturbance of the scale assumed and since that ϵ is small, the exponent of the first term of Eq. (3.45) is uniformly smaller than the argument of the final exponential for $\epsilon\chi$, $t = O(1)$. If the nature of the initial singularity in Eq.

(3.43) were different, it would make little difference since the first exponential term would be one again, though a different choice would modify the *algebraic* factor in Eq. (3.45). [For example, a second-order pole instead of Eq. (3.43) produces a result essentially like Eq. (3.45), except that the $\xi_d^{1/4}$ multiplier becomes $\xi_d^{3/4}$; the final exponential is of course unchanged.] Thus, to a large degree, the result for growth rate according to linear theory is independent of the detailed nature of initial disturbance (or, more precisely, the nature of the complex singularity). Such a conclusion is, as we shall see later, qualitatively different from what is to be found for the nonlinear equations.

A few other comments are in order before proceeding to the next subsection in which we develop a deeper understanding of the solution behavior (3.45). Notice that even though the disturbance starts being confined to an $O(\epsilon)$ neighborhood in ξ close to the tip, by the time the long-time behavior given in Eq. (3.45) is appropriate, the disturbance is of width $O(1)$ at least, since χ always appears in Eq. (3.45) in the combination $\epsilon\chi$. The boundary layer analysis is still valid formally because it requires only $\epsilon\chi \ll \xi_d$, and since ξ_d is large, this condition is satisfied. However, the result also shows that the disturbance can have a large spatial extent compared to the tip radius, while not failing to be small compared to the distance from the tip. Also, we note that as $t \to \infty$, the local wavelength of the oscillations present in the solution (3.45) scales as $(\mathcal{B}/\xi_d)^{1/2}$, which becomes shorter with time. This is not consistent with sidebranch coarsening observed in experiment.

For purposes of comparison of our results with other works, for $\xi_d \gg 1$, we replace ξ_d everywhere by $(-2y_d)^{1/2}$, where y_d is the y location of the disturbance in the tip frame of the dendrite. We also replace M by 1. Then the shape of the distorted interface is given approximately by

$$y \sim -\frac{x^2}{2} + \mathrm{Im}(Z^1|_{\xi_d = \sqrt{-2y_d}}), \qquad (3.46)$$

which is essentially the same result as given in Eq. (5.5) of Barber, Barbieri, and Langer [16], except, as noted, the algebraic attenuation factor $(1 + i\epsilon\chi)^{-1/4}$ is missing in their results.

B. Linear dynamics in the complex plane

An alternate approach to understanding wave-packet dynamics involves studying the dynamical equations in the complex lower-half ζ plane. For the linear problem itself, the advantages of such an approach are limited; nonetheless, the ensuing discussion of the linear complex plane dynamics is useful in understanding how approaching complex singularities can correspond to the intensification and lateral spreading of an initially confined disturbance: a connection that transcends linearity, as we will show in later sections. In fact, it is only in the light of this analysis of singularity motion in the lower-half ζ plane that results like Eq. (3.31) can be properly understood.

In this section, we consider the linearized dynamical equation (3.17), which is valid only under rather restricted conditions. We consider the analytic continuation of the initial condition $Z^1(\zeta, 0)$ to the lower-half complex ζ plane. It is

well known in complex variables that this process of analytic continuation is not well posed. In other words, if the interfacial shape is provided to a finite nonzero error in an experiment or simulation, then the extension of $z^1(\zeta, 0)$ into the lower half plane cannot be uniquely determined in any meaningful manner.

The evolution of the dendrite corresponding to very different initial conditions in the complex plane may correspond to nearly identical initial conditions in the laboratory. For example, let $z_1^1(\zeta, 0)$ be one particular initial condition and let $z_2^1(\zeta, 0) = z_1^1(\zeta, 0) + \delta_1/(\zeta + i\delta_2)$ with $\delta_2 > 0$ be another initial condition. These two differ on the real ζ axis by a small amount for $|\delta_1|/\delta_2$ sufficiently small, meaning that the interfacial shapes in the two cases are nearly identical. Yet z_1^1 and z_2^1 differ by a large, singular amount in the lower-half complex plane. This latter difference leads to significantly different interfacial distortions at *later* times as the complex singularities continually approach the real axis from below: as we shall soon see that they do. Therefore, by beginning with a known singularity distribution in the complex plane rather than with a known interface position, this sensitivity to initial condition is removed. Experimental observations are then understood in terms of an ensemble of complex singularity distributions subject to the requirement that the interfacial shape corresponding to any one of a number of complex initial conditions are indistinguishable to within experimental error.

We now focus on a single isolated complex singularity $\zeta_s(0)$ of $Z^1(\zeta, 0)$ in the lower-half plane. We ignore anisotropy effects in this analysis since the results from Sec. II A indicate that anisotropy has no effect on the results for asymptotic growth rate far from the tip. The analytic continuation of the dynamical equation (3.17) for $\alpha = 0$ to the lower-half plane is given by

$$Z_t^1 = q_1^0 Z_\zeta^1 - \frac{i\mathcal{B}}{[z_\zeta^0 \tilde{z}_\zeta^0]^{3/2}} Z_{\zeta\zeta\zeta}^1, \qquad (3.47)$$

$\tilde{z}^0$ is a locally analytic function that is equal to the complex conjugate z^{0*} on the real axis, and $q_1^0(\zeta, t)$ is an analytic function in the lower-half complex ζ plane, defined by

$$q_1^0(\zeta, t) = \frac{1}{\pi} \int_{-\infty}^{\infty} d\xi \, \frac{R^0(\xi, t)}{\xi - \zeta}, \qquad (3.48)$$

where R^0 is as defined in Eq. (3.3). It is clear from the Plemelj formula that as ζ approaches the real axis from below,

$$q_1^0 \to H_0 - iR_0. \qquad (3.49)$$

Further, it is clear that on the real axis $|z_\zeta^0|^2 = z_\zeta^0 \tilde{z}_\zeta^0$. Thus Eq. (3.47) is easily seen to be the analytic continuation of Eq. (3.17) (with $\alpha = 0$) to the lower-half complex plane. It is to be noted that if we substitute $z_\zeta^0 = 1 - i\zeta$, as appropriate for the Ivantsov solution, the corresponding q_1^0 can be evaluated exactly to be

$$q_1^0 = -\frac{1}{\zeta - i}. \qquad (3.50)$$

In general, if $z^0_\zeta = O(\zeta)$ for $|\zeta| \gg 1$,

$$q^0_1(\zeta,t) \sim -\frac{M}{\zeta} + O(\zeta^{-2}), \qquad (3.51)$$

where M is once again determined as in Eq. (3.34). Note from Eqs. (3.49) and (3.50) that for the Ivantsov solution $M=1$ and that this value is approached for a steady base state for $\mathcal{B} \neq 0$ for small anisotropy α. First, if we neglect surface energy $\mathcal{B}$ in Eq. (3.47), it is clear that

$$Z^1(\zeta,t) = Z^1(\nu,0), \qquad (3.52)$$

where the relation ν as a function of (ζ,t) is determined by solving the characteristic equation

$$\dot{\zeta} = -q^0_1(\zeta(t),t) \quad \text{where} \quad \zeta(0) = \nu. \qquad (3.53)$$

Therefore, according to Eq. (3.52), whatever structure characterizes Z^1 initially, that structure ''advects'' along a path given by the solution to Eq. (3.53). We note that $\mathrm{Im}q^0_1(\zeta,t)$ is a harmonic function in the lower-half plane in the ξ-η variable, taking on the value $-R_0(\zeta,t) < 0$ on the boundary (ξ axis, i.e., real ζ axis). From a maximum principle, $\mathrm{Im}q^0_1 < 0$ everywhere in the lower-half plane. Thus $\mathrm{Im}\dot\zeta = \dot\eta > 0$, which implies that for $t > 0$, for any ζ on the real axis, the corresponding ν satisfies the relation $\mathrm{Im}\nu < 0$. Therefore, the isolated $Z^1(\zeta,0)$ structure that begins in the lower-half complex ζ plane propagates to the real axis in a finite time and perhaps crosses the axis. In particular, if the initial data $Z^1(\zeta,0)$ happen to have a singularity at $\zeta = \zeta_s(0)$, where $\mathrm{Im}\zeta_s(0) < 0$, then the singularity $\zeta_s(t)$ will propagate toward and hit the real axis at a finite time. In the special case where the background state is the Ivantsov solution (for $\mathcal{B}=0$) $z^0_\zeta = 1 - i\zeta$, the trajectory of the singularity (in this case) is

$$\zeta_s(t) = i + \sqrt{[\zeta_s(0) - i]^2 + 2t}. \qquad (3.54)$$

Note, in this case, that this singularity in the lower-half plane hits the real ζ axis before eventually approaching $\mathrm{Im}\zeta_s = 1$. When $\mathrm{Re}\zeta_s(0) > 0$, it is clear that $\mathrm{Re}\zeta_s = \xi_s \to +\infty$ as $t \to \infty$ and that for $\mathrm{Re}\zeta_s(0) < 0$, $\mathrm{Re}\zeta_s(t) = \xi_s(t) \to -\infty$.

While the solution ceases to make physical sense beyond the time when $\mathrm{Im}\zeta_s(t) = 0$ for $\mathcal{B} \equiv 0$, the same is not true for any nonzero $\mathcal{B}$, however small. As we shall soon discover, the zero-surface-energy singularity located at $\zeta_s(t)$ is replaced by a smoothed out inner structure centered at $\zeta_s(t)$. In such cases, it is necessary to compute the trajectory $\zeta_s(t)$ even as it enters the upper-half plane. This inner structure affects the solution on the real ζ axis and hence the interface shape, even when it is well into the upper-half plane. To study the trajectory of $\zeta_s(t)$, we need to write down the analytic continuation of $q^0_1(\zeta,t)$, as it is defined in Eq. (3.48), from the lower-half plane to the upper-half plane. Recall that the analytic continuation of $|z^0_\zeta|^2$ off the real axis is $z^0_\zeta \bar{z}^0_\zeta$, while that of $\mathrm{Im}\omega^0_\zeta$ is given by $(\omega^0_\zeta - \tilde\omega^0_\zeta)/2i$. Thus, for $\zeta_s(t)$ in the upper-half plane, Eq. (3.48) implies that

$$\dot\zeta_s = -q^u_0(\zeta_s(t),t) + 2i\frac{[1 - (\mathcal{B}/2i)(\omega^0_\zeta - \tilde\omega^0_\zeta)]}{z^0_\zeta \bar{z}^0_\zeta}, \qquad (3.55)$$

where

$$q^u_0(\zeta,t) = \frac{1}{\pi}\int_{-\infty}^{\infty}\frac{d\xi}{\xi - \zeta}R^0(\xi,t). \qquad (3.56)$$

Note that even though the expressions for q^0_1 and q^u_0 are identical, they are not the same analytic functions; q^0_1 is defined with the integral expression (3.48) only when $\mathrm{Im}\zeta_s < 0$, whereas the above definition of $q^u_0(\zeta_s,t)$ is valid only when $\mathrm{Im}\zeta_s > 0$. Indeed, on the real ζ axis, the Plemelj formula implies that $q^u_0 - q^0_1 = 2iR^0$.

Now, we consider separately the equations for $\xi_s(t)$ and $\eta_s(t)$, the real and imaginary parts of $\zeta_s(t)$, in the case the $t \gg 1$. Since we have noted in Sec. III A that for $|\zeta| \gg 1$, $z_\zeta \sim -i\zeta$, then $\tilde{z}_\zeta \sim +i\zeta$. Further, for large $|\zeta|$, Eq. (3.27) is approximated by

$$\omega^0_\zeta \sim \frac{1}{\pi i \zeta^2}\int_{-\infty}^{\infty}K_0(\xi,t)d\xi. \qquad (3.57)$$

Therefore, in the absence of an essential singularity at ∞,

$$\tilde\omega^0_\zeta \sim -\frac{1}{\pi i \zeta^2}\int_{-\infty}^{\infty}K_0(\xi,t)d\xi. \qquad (3.58)$$

From Eqs. (3.55), (3.58), and (3.59), $q^u_0 \sim q^0_1 + o(\xi_s^{-2})$. Thus, taking the real part of Eq. (3.55) leads to the long-time differential equation for ξ_s,

$$\dot\xi_s(t) \sim \frac{M}{\xi_s(t)} + O(\xi_s^{-2}), \qquad (3.59)$$

from which we trivially obtain

$$\xi_s(t) \sim \sqrt{\int^t 2M\,dt}. \qquad (3.60)$$

When M approaches a constant as $t \to \infty$ then $\xi_s(t) \sim \sqrt{2Mt}$.

On taking the imaginary part of Eq. (3.55), we obtain

$$\dot\eta_s = -\frac{1}{\pi}\int_{-\infty}^{\infty}\frac{\eta_s}{(\xi - \xi_s)^2 + \eta_s^2}R^0(\xi,t)d\xi$$
$$+ 2\,\mathrm{Re}[R^0(\zeta_s(t),t)], \qquad (3.61)$$

where $R^0(\zeta,t)$ is now the analytic continuation of the expression for $R^0(\xi,t)$ off the real ζ axis and is given by

$$R^0(\zeta,t) \sim \frac{1}{z^0_\zeta \bar{z}^0_\zeta}\left[1 - \frac{\mathcal{B}}{2i}(\omega^0_\zeta - \tilde\omega^0_\zeta)\right]. \qquad (3.62)$$

Consider the large-t behavior of the integral in Eq. (3.61) by breaking it into

$$\int_{-\infty}^{-L} + \int_{-L}^{L} + \int_{L}^{\xi-L} + \int_{\xi-L}^{\xi+L} + \int_{\xi+L}^{\infty}, \qquad (3.63)$$

where $\eta_s \ll L \ll \xi_s$ and $L \gg 1$. By substituting $\xi = \xi_s\nu$ in the first-integral and using $R^0(\nu\xi_s,t) = O(\xi_s^{-2}\nu^{-2})$, it follows that the contribution from each of $\int_{-\infty}^{-L}$, $\int_{L}^{\xi_s-L}$, and $\int_{\xi_s+L}^{\infty}$ is
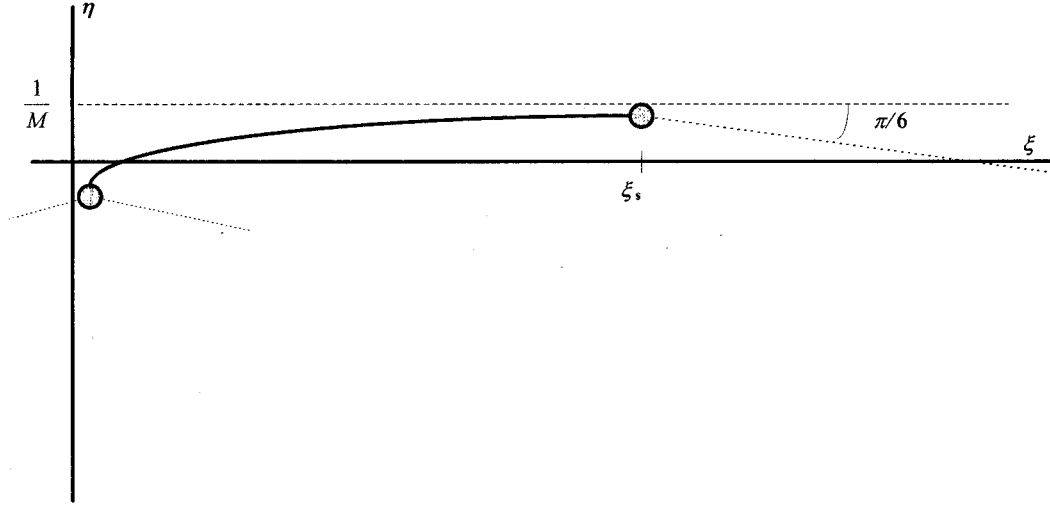
FIG. 4. ζ-plane trajectory of a singularity across the real axis and into Im$\zeta > 0$, according to linearized analysis. Shown schematically is the singularity at $t = 0$ and for large times when the singularity is in the upper-half ζ plane. The dashed lines are the Stokes lines that bound the downward-facing wedge in which the solution is temporally growing and spatially oscillatory.

$O(\eta_s \xi^{-2} L^{-1})$. Of the remaining integral, $\int_{-L}^{L}$ clearly contributes $-M \eta_s / \xi_s^2$ as $L \to \infty$, while on substituting $\xi - \xi_s = \eta_s \nu$, it is clear that $\int_{\xi_s - L}^{\xi_s + L}$ contributes an additional $-R^0(\xi_s, t)$. If the far-field behavior of $z_\zeta^0 \sim -i\zeta$ and $\bar{z}_\zeta^0 \sim -i\zeta$ is valid, it follows that the last term in Eq. (3.61) contributes $2R^0(\xi_s(t), t)$. Adding all together, we obtain

$$\dot{\eta}_s \sim -\frac{M \eta_s}{\xi_s^2} + R^0(\xi_s(t), t). \tag{3.64}$$

Integrating,

$$\eta_s \sim \frac{1}{\xi_s(t)} \int^t dt' R^0(\xi_s(t'), t') \xi_s(t'). \tag{3.65}$$

If $M(t)$ approaches a constant as $t \to \infty$ and $\xi_s(t)$ is large enough so that the approximation $R^0(\xi_s(t), t) \sim \xi_s^{-2}$ holds, it follows that

$$\eta_s \to \frac{1}{M} \quad \text{as } t \to \infty. \tag{3.66}$$

Now we move on to extend the analysis to include nonzero surface energy $\mathcal{B}$ in Eq. (3.47). For now on we concentrate on an inner neighborhood of the singularity $\zeta_s(t)$ that moves according to Eq. (3.53). We introduce the local variable

$$\zeta = \zeta_s(t) + \exp\left[-\int_0^t q_{1_\zeta}^0(\zeta_s(t), t)\right] \mathcal{B}^{1/3} \chi. \tag{3.67}$$

It is convenient to define $Q^0(t)$ so that

$$\ln Q^0(t) = -\int_0^t q_{1_\zeta}^0(\zeta_s(t), t) dt. \tag{3.68}$$

It is clear that $Q^0(0) = 1$. Further, the asymptotics of $q_1^0 \sim -M/\zeta$ and the trajectory equation $\dot{\zeta}_s = -q_1^0(\zeta_s(t), t)$ show that for $t \gg 1$ (and hence $|\zeta_s| \gg 1$)

$$Q^0(t) \sim \frac{C}{\zeta_s(t)}, \tag{3.69}$$

where C is some constant. Using definition, Eq. (3.67) can be rewritten as

$$\zeta = \zeta_s(t) + Q^0(t) \mathcal{B}^{1/3} \tilde{\chi}. \tag{3.70}$$

Notice that the quantity $\tilde{\chi}$ used here differs from the χ of Sec. III A; in fact, $\chi = \tilde{\chi} Q^0(t)$. We define a rescaled time variable

$$\tau = -i \int_0^t [z_\zeta^0(\zeta_s(t'), t')]^{-3/2} [\bar{z}_\zeta^0(\zeta_s(t'), t')]^{-3/2}$$

$$\times \frac{1}{[Q^0(t')]^3} dt'. \tag{3.71}$$

If ξ_s is sufficiently far along the real axis so that $z_\zeta^0(\zeta_s(t), t) \sim -i\zeta_s$ (i.e., is close to the Ivantsov solution), it follows that in the special case where $|\zeta_s(t)| \gg 1$ for all t, we can write Eq. (3.71) as

$$\tau \sim -\frac{it}{C^3}. \tag{3.72}$$

Note from Eq. (3.71) that $\arg(\tau)$ is initially close to $-\pi/2$, since $|\text{Im} \eta_s(0)| \ll 1$, and so $\arg[z_\zeta \bar{z}_\zeta]$ is close to zero and $Q(0) = 1$. If we define

$$Z^1(\zeta(\tilde{\chi}, t(\tau)), t(\tau)) = G(\tilde{\chi}, \tau), \tag{3.73}$$

the leading-order equation for G derived from Eq. (3.17) is simply

$$G_\tau = G_{\tilde{\chi}\tilde{\chi}\tilde{\chi}}. \tag{3.74}$$

The solution to Eq. (3.74) that matches $G(\chi,0)$ when $t\rightarrow0^{+}$ for $\arg(\xi)$ in the interval $(-\pi/6,\ 7\pi/6)$ (a range of argument that includes the solution on the real χ axis) is

$$G(\widetilde{\chi},\tau)=\frac{1}{2\pi}\int_{-\infty}^{\infty}d\widetilde{\chi}'\,G(\widetilde{\chi}',0)(\widetilde{\chi}-\widetilde{\chi}')^{1/2}\tau^{-1/2}F$$
$$\times(-i(\widetilde{\chi}-\widetilde{\chi}')^{3/2}/\tau^{1/2}),\qquad(3.75)$$

where the integral is to be interpreted along the real $\widetilde{\chi}'$ axis though it skirts just above the initial singularity at $\widetilde{\chi}'=0$, and

$$F(\beta)=\int_{C}dx\ e^{-\beta x(1-x^{2})},\qquad(3.76)$$

where C is a straight-line contour from $x=0$ to ∞ along a ray determined by $\arg(x)=-\pi/3-\frac{1}{3}\arg(\beta)$. It is easily seen that $F(\beta)$ defines an analytic function for all finite complex β, except $\beta=0$, where it has the asymptotic behavior

$$F(\beta)\sim\frac{e^{-i\pi/3}\Gamma(\frac{1}{3})}{3\beta^{1/3}}.\qquad(3.77)$$

The asymptotic behavior of the solution (3.76) for $\beta\rightarrow\infty$ involves contributions from a saddle point in the x plane and also the contribution from the vicinity of the end point at $x=0$. Which is dominant depends on the argument of β, and the entire process must be done with great care. For $\arg(\beta)$ in the interval $[-\pi/2,\ 3(\pi/2)]$, the end point dominates and so

$$F(\beta)\sim\frac{1}{\beta}.\qquad(3.78)$$

In other regimes in $\arg(\beta)$, however, a saddle-point contribution is dominant. Thus, for $\arg(\beta)$ in the interval $(-2\pi,\ -\pi/2)$,

$$F(\beta)\sim-i\sqrt{\frac{\pi}{3^{1/2}\beta}}\,e^{-2\beta/3\sqrt{3}}[1+O(\beta^{-1})],\quad(3.79)$$

while for $\arg(\beta)$ in the interval $(3\pi/2,\ 2\pi)$,

$$F(\beta)\sim\sqrt{\frac{\pi}{3^{1/2}\beta}}\,e^{2\beta/3\sqrt{3}}.\qquad(3.80)$$

With the known asymptotic behavior stated in Eq. (3.78) in the given sector and the relation $\arg(\beta)\sim-\pi/4+\frac{3}{2}\arg(\widetilde{\chi}-\widetilde{\chi}')$, which is valid at least for $t\ll1$, it follows that as $t\rightarrow0^{+}$, with $\arg(\zeta-\zeta_{s})$ in the $(-\pi/6,\ 7\pi/6)$ the integral in Eq. (3.75) simplifies to

$$\frac{1}{2\pi i}\int_{-\infty}^{\infty}\frac{d\widetilde{\chi}'}{\widetilde{\chi}'-\widetilde{\chi}}G(\widetilde{\chi}',0)=G(\widetilde{\chi},0)$$

since $Z^{1}(\xi,0)$ and hence $G(\widetilde{\chi},0)$ is analytic in the upper-half plane (including at infinity). Thus the solution (3.75) does indeed satisfy the initial condition on the real ξ axis. In the special case when $Z^{1}(\zeta,0)=\delta/[\zeta-\zeta_{s}(0)]$,

$$G(\widetilde{\chi},0)=\frac{A}{\widetilde{\chi}}\quad\text{with }A=\delta\mathcal{B}^{=1/3}.\qquad(3.81a)$$

However, this evaluation of $G(\widetilde{\chi},0)$ must also, for short times, contain within it the large χ behavior of G, and in order for this solution to match to the required far-field form $G\sim A/\chi$, $\chi\rightarrow\infty$ (see argument below), we must write, instead of Eq. (3.81a),

$$G(\widetilde{\chi},0)=\frac{A}{\chi}=\frac{A'}{\widetilde{\chi}},\quad A'\equiv A/Q^{0}(t).\qquad(3.81b)$$

Equation (3.75), at least for t sufficiently small, simplifies to

$$G(\widetilde{\chi},\tau)=-iA'\widetilde{\chi}^{1/2}\tau^{-1/2}F(-i\widetilde{\chi}^{3/2}/\tau^{1/2}).\qquad(3.82)$$

To see this result, we have to note that we can close the contour in the $\widetilde{\chi}'$ plane with a large semicircle in the lower-half plane so that on the large lower-half semicircular arc $\arg(\widetilde{\chi}-\widetilde{\chi}')$ is in the interval $(0,\pi)$ for which the corresponding $\arg(\beta)$ is within the interval where the behavior (3.78) is valid. This means that there is no contribution from this large semicircular arc and the only contribution to a contour-integral evaluation of Eq. (3.75) comes from the residue at $\widetilde{\chi}'=0$, which results in Eq. (3.82). Actually, it is directly possible to verify that Eq. (3.82) is a solution to Eq. (3.74), satisfying the condition that as $t\rightarrow0$, $G(\widetilde{\chi},\tau)\rightarrow A'/\widetilde{\chi}$ for any fixed $\widetilde{\chi}\neq0$, provided $\arg(\widetilde{\chi})$ (and therefore $\arg[\zeta-\zeta_{s}(0)]$) is in the interval $(-\pi/6,\ 7\pi/6)$, which includes the real ζ axis that corresponds to the physical interface. However, because of the sectorial nature of the asymptotic (3.78)–(3.80), it is evident that as $t\rightarrow0+$, $G(\widetilde{\chi},\tau)$ does not tend to the initial condition (3.81) as $\tau\rightarrow0+$ in certain sectors in the lower-half complex ζ plane. Because of the equivalence of large $\widetilde{\chi}$ and small τ in the similarity variable

$$\beta=-i\frac{\widetilde{\chi}^{3/2}}{\tau^{1/2}},\qquad(3.83)$$

it follows that for any $t>0$, as $\widetilde{\chi}\rightarrow\infty$, the zero-surface-energy behavior $G(\widetilde{\chi},\tau)\sim1/\widetilde{\chi}$ is not recovered, except in certain sectors of the complex plane. Instead using Eq. (3.79), we obtain

$$G(\widetilde{\chi},\tau)\sim-i\frac{A'}{\widetilde{\chi}}\sqrt{\frac{\pi\beta}{3^{1/2}}}\,e^{-2\beta/3\sqrt{3}},\qquad(3.84)$$

when $\arg(\beta)$ is in the interval $(-2\pi,\ -\pi/2)$ and

$$G(\widetilde{\chi},\tau)\sim\frac{A'}{\widetilde{\chi}}\sqrt{\frac{\pi\beta}{3^{1/2}}}\,e^{2\beta/3\sqrt{3}},\qquad(3.85)$$

when $\arg(\beta)$ is in the interval $(3\pi/2,\ 2\pi)$, corresponding to an exponential-oscillatory behavior. For sufficiently large t, when $\xi_{s}(t)$ is large enough so that Eqs. (3.69) and (3.71) hold, we obtain from Eqs. (3.70) and (3.83) that

$$\beta\sim\frac{e^{-i\pi/4}}{\mathcal{B}^{1/2}t^{1/2}}\zeta_{s}^{3/2}[\zeta-\zeta_{s}(t)]^{3/2}.\qquad(3.86)$$

The asymptotic behavior of G then depends upon the sector, as noted. If β lies in the interval $(-\pi/2,\ 3\pi/2)$ [which corresponds to $\arg(\chi)$ in the interval $(-\pi/6,\ 7\pi/6)$,] then we recover Eq. (3.81a) as the solution for long times. However, as the singularity moves into $\text{Im}\zeta>0$, a large segment

of the real axis is not in that sector (see Fig. 4). In fact, for that part of the real axis for which $\arg(\xi-\zeta_s)$ is in the interval $(-7\pi/6, -\pi/6)$, Eq. (3.85) gives the Z^1 behavior

$$Z^1(\xi,t) \sim -i\delta\left(\frac{\pi^2\xi_s^3}{3\mathcal{B}t[\eta_s+i(\xi-\xi_s)]}\right)^{1/4}$$
$$\times \exp\left[\frac{2}{3}\sqrt{\frac{\xi_s^3}{3\mathcal{B}t}}[\eta_s+i(\xi-\xi_s)]^{3/2}\right].$$

(3.87)

The reader is reminded that this asymptotic solution is valid for short times and/or large values of $\chi-\chi_s$ and so the apparent branch-point singularity in Eq. (3.87) is in fact not there since Eq. (3.77) shows that, as $\chi-\chi_s\to 0$, the behavior is, in fact, $1/(\chi-\chi_s)$. When M asymptotically approaches a constant for large t, then $\xi_s\sim\sqrt{2Mt}$, $\eta_s\sim 1/M$, and the above expression for Z^1 simplifies to

$$Z^1(\xi,t) \sim -i\delta\left(\frac{2\pi^2M^2\xi_s}{3\mathcal{B}[1+iM(\xi-\xi_s)]}\right)^{1/4}$$
$$\times \exp\left[\frac{2}{3M}\sqrt{\frac{2\xi_s}{3\mathcal{B}}}[1+iM(\xi-\xi_s)]^{3/2}\right].$$

(3.88)

It should be noted that Eq. (3.88) recovers precisely the linearized, real-domain analysis of Sec. III A, in particular Eq. (3.45). Notice, however, that we can understand from Eq. (3.88), in terms of its domain of validity, how to properly regard the results of Sec. III A. Since $\arg[1+iM(\xi-\xi_s)]=\pi/3$ corresponds to $\arg(\beta)=-\pi/2$, when $\xi=\xi_s+\sqrt{3}/M$, the oscillatory behavior given by Eq. (3.88) is confined to $\xi<\xi_s+\sqrt{3}/M$. (Note the right-hand dashed line in Fig. 4.) Ahead of it, there is no effect of the singularity. Behind it, there is a trail of a wave train. From the above results, it might appear that the wave train extends all the way to point $\xi=\xi_{\text{impact}}$, near $\xi=0$, where the singularity $\zeta_s(t)$ first crossed over to the upper-half plane. However, this conclusion cannot be verified by the analysis presented here since it requires $|\xi-\xi_s|\ll\xi_s$, which would not be satisfied if we move far from $\xi=\xi_s$ towards the tip region. In fact, what happens is this: While the singularity center is in $\text{Im}\zeta<0$, the angles from that center to locations on the real axis lie in $(0,\pi)$. However, as the singularity crosses the real axis, those angles, for some values of ξ, fall below $-\pi/6$ on the right and approach $-\pi$ at the left, so that the asymptotic approximation (3.84) becomes appropriate for all of the real axis in the neighborhood of the singularity. Obviously, as noted, far to the left, where the value of $\arg(\widetilde{\chi})$ is near $-\pi$, the singularity trajectory track is so far from the singularity as to make the asymptotics incorrect, so that we can say nothing about the character of the singularity "wake" in this region. So the conclusions from the linearized analysis, when properly understood in the complex domain, are as follows.

(i) An initially confined disturbance near the tip (starting near the imaginary axis in Fig. 4) creates a very large, growing wavelike structure, which may be small compared to the distance from its starting location ($|\xi-\xi_s|\ll\xi_s$), but is in fact very large compared to, say, the tip radius. The wavelike structure is a direct consequence of a zero-surface-energy singularity crossing over into $\text{Im}\zeta>0$, thus exposing the Stokes phenomenon behind the regularized structure of the singularity.

(ii) The form of the long-time behavior for a singularity is only weakly dependent on the nature of the complex singularity in $\text{Im}\zeta<0$, associated with the initially confined disturbance.

(iii) The spatial growth rate is like $\exp(\text{const}\times t^{1/4})$.

It is incumbent on us to pursue the fully nonlinear problem in the complex plane to explore how, in fact, such initial singularities behave as they near the real axis from below. The linearized-analysis crossover may be atypical and misleading. To anticipate our nonlinear results as they relate to the items listed above, we will find that, in fact, (i) the interaction of the singularity with the real axis, whether it crosses over, hits, or asymptotically approaches the axis, is dependent on the singularity character: there is no generic behavior for all singularities (and zeros); (ii) for a class of disturbances associated with specific types of initial singularities in $\text{Im}\zeta<0$, the spatial growth rate of the local conformal map is like $\exp(\text{const}\times t^{1/2})$.

Now we turn to the fully nonlinear problem in the complex ζ plane.

IV. NONLINEAR COMPLEX PLANE EQUATIONS

We noted in Sec. III, at least in the context of linear equations, how complex singularities approaching the real axis affect the evolution of the dendrite interface. The motion of singularities in the complex plane according to the zero-surface-energy equation was shown to be relevant to understanding the time-evolving behavior of a superposed disturbance, even when nonzero-surface-energy effects are included. Indeed, the zero-surface-energy advection of singularities was found to be crucial in both the qualitative and quantitative aspects of amplification of noise and sensitivity of dynamics to initial conditions.

It can be expected that with inclusion of nonlinear effects, the linear dynamics described in Sec. III will be modified. A very important part of this modification occurs due to the differences between linear and nonlinear motion of zero-surface-energy singularities, and this will be investigated in detail in this and later sections. In addition, the class of zero-surface-energy solutions is very broad and shows a whole range of interfacial phenomena, including tip splitting, side-branching, coarsening, and cusp formation. However, as we already know in the context of Hele-Shaw motion for isotropic surface energy and from what will be described in the companion papers for the dendrite and Hele-Shaw flow with anisotropy, not all the zero-surface-energy solutions are possible limits of solutions as surface energy tends to zero. The understanding of the singular perturbation effects of surface energy is effected through the complex plane dynamics, where the zero-surface-energy dynamics is well posed. The starting point of the complex plane dynamics is once again the zero-surface-energy equation, analytically continued to the lower-half plane.

In this section we take the region I equations with $\mathcal{B}=0$ and modify them through analytic continuation to the lower-half plane in order to define a well-posed evolution problem similar to that for the Hele-Shaw problem (see Ref. [37]). We then examine some of the general properties of the gov-

erning equations. Many of these properties follow from earlier studies on the mathematically related Hele-Shaw flow [34] and will be quoted without details. We note that the zero-surface-energy problem is valid for both the one-sided diffusion model explicitly being investigated and the two-sided diffusion model with nonzero thermal diffusion in the solid.

Unlike Sec. II, it is now more convenient to work in the laboratory frame of reference, so from Eq. (2.28) we find that the $\mathcal{B}=0$ governing equation in the upper-half plane is

$$z_t = q_1(\zeta,t)z_\zeta, \qquad (4.1)$$

where

$$q_1(\zeta,t) = \frac{1}{\pi}\int_{-\infty}^{+\infty}\frac{d\xi'}{\xi'-\xi}\frac{1}{|z_\zeta(\xi',t)|^2}$$

$$= \frac{1}{\pi}\int_{-\infty}^{+\infty}\frac{d\xi'}{\xi'-\zeta}\frac{1}{z_\zeta(\xi',t)\widetilde{z}_\zeta(\xi',t)}, \qquad (4.2)$$

and as in Sec. III B, we use (cf. Ref. [34])

$$\widetilde{z}_\zeta(\zeta,t) \equiv (z_\zeta(\zeta^*,t))^*, \qquad (4.3)$$

which is a function analytic in the lower-half plane equaling the complex conjugate of z_ζ on the real axis. Upon analytic continuation (see, for instance [42], for the procedure via contour deformation), we find the equation for the lower-half plane to be

$$z_t = q_1(\zeta,t)z_\zeta + q_2(\zeta,t), \qquad (4.4)$$

$$q_2(\zeta,t) = \frac{2i}{\widetilde{z}_\zeta(\zeta,t)}. \qquad (4.5)$$

We note that while Eq. (4.4) is a nonlinear integro-differential equation, with q_1 and q_2 depending on z, both q_1 and q_2 define analytic functions of ζ for $\mathrm{Im}(\zeta)<0$, as long as an analytic solution exists on the real domain. This *a priori* information of analyticity of q_1 and q_2 implies that z in the lower-half complex plane, satisfying Eq. (4.4), has the property of the solution of a linear hyperbolic equation with analytic coefficients [43]. In particular, no singularities of z are spontaneously created in the lower-half plane. The ones present initially move with characteristic speed $d\zeta/dt = -q_1$, which depends globally on the solution z through the integrand in q_1. From expression (4.2) it follows that $\mathrm{Im}q_1$ is a harmonic function everywhere in the lower-half plane (including infinity), taking on boundary values

$$\mathrm{Im}q_1 = -\frac{1}{|z_\zeta|^2}. \qquad (4.6)$$

From the maximum principle for a harmonic function, it follows that

$$\mathrm{Im}q_1 < 0 \qquad (4.7)$$

everywhere in the lower-half plane. This implies that

$$\mathrm{Im}\dot{\zeta}_s > 0, \qquad (4.8)$$

and so every singularity initially present in the lower-half plane advects towards the real axis, a property first shown in the context of the Hele-Shaw flow [34].

We now consider special initial conditions of the form

$$z(\zeta,0) = G(\zeta,0) + \sum_{j=1}^{N} E_J(\zeta,0)\frac{[\zeta-\zeta_{sj}(0)]^{1-\beta_j}}{1-\beta_j}, \quad (4.9)$$

$$G(\zeta,0) = -\frac{i}{2}\zeta^2 + \zeta, \qquad (4.10)$$

where Eq. (4.10) is the underlying Ivantsov parabola at initial time. The initial conditions for E_j and ζ_{sj} and the exponents β_j are specified. When $\beta_j=1$, we replace the expression $[\zeta-\zeta_{sj}(0)]^{1-\beta_J}/(1-\beta_j)$ by $\ln[\zeta-\zeta_{sj}(0)]$. Following arguments presented in [34] and [37] it follows that

$$z(\zeta,t) = G(\zeta,t) + \sum_{J=1}^{N} E_j(\zeta,t)\frac{[\zeta-\zeta_{sj}(t)]^{1-\beta_j}}{1-\beta_j}, \qquad (4.11)$$

where G and E_j are analytic in the lower-half ζ plane and satisfy

$$G_t = q_1(\zeta,t)G_\zeta + q_2(\zeta,t), \qquad (4.12)$$

$$(E_j)_t = q_1(\zeta,t)(E_j)_\zeta + (1-\beta_j)\frac{q_1(\zeta,t)-q_1(\zeta_{sj}(t),t)}{\zeta-\zeta_{sj}(t)}E_j, \qquad (4.13)$$

where

$$\dot{\zeta}_{sj} = -q_1(\zeta_{sJ}(t),t). \qquad (4.14)$$

It follows that

$$G(\zeta,t) = -\frac{i}{2}\zeta^2 + \zeta + b_0(t), \qquad (4.15)$$

$$\dot{b}_0(t) = \frac{i}{\pi}\int_{-\infty}^{+\infty}\frac{d\xi'}{|z_\zeta(\xi',t)|^2}, \quad b_0(0)=0. \quad (4.16)$$

In the case of no initial singularities, $b_0(t)=it$ and G is the Ivantsov solution in the laboratory frame, as we should expect.

In the vicinity of the singularity ζ_{sj}, it is clear that

$$E(\zeta,t) \sim E_0(t) + O(\zeta-\zeta_s),$$

where

$$E_0(t) = E_0(0)\exp\left((1-\beta)\int_0^t dt' q_{1\zeta}(\zeta_s(t'),t')\right). \quad (4.17)$$

Note that if $\beta=1$, then $E_0(t)$ is a constant.

Given that all singularities will approach the real axis, we are interested in the behavior of a singularity as it nears that axis. Consider the neighborhood of a singularity that is near the real axis

$$z_\zeta \sim \begin{cases} A_0(t) + E_0(t)[\zeta-\zeta_s(t)]^{-\beta}, & \beta<0 \\ E_0(t)[\zeta-\zeta_s(t)]^{-\beta}, & \beta>0, \end{cases} \quad (4.18)$$

with $0 < -\eta_s \ll 1$. The factor $E_0(t)$ is known from Eq. (4.17) and $A_0(t)$ is the local behavior from every other part of the conformal map. We study the behavior of $\zeta_s(t)$ by looking at its governing equation (4.14) in the limit of $\eta_s \to 0 -$, in a fashion similar to that of Tanveer [34]. First, we separate the real and imaginary components of Eq. (4.14) and break up each integral into an inner contribution adjacent to the singularity where $|\xi' - \xi_s(t)| \leq \epsilon$ [ϵ being a convenient constant $-\eta_s(t) \ll \epsilon \ll 1$, which the final result is independent of] and outer contributions. [The process is similar to that detailed in Eq. (2.33) and following arguments.] By comparing the various inner and outer contributions, we find the real part of the singularity behavior to be governed by

$$\dot{\xi}_s(t) \sim -\frac{1}{\pi} \fint_{-\infty}^{+\infty} \frac{d\xi'}{\xi' - \xi_s(t)} \frac{1}{|z_\zeta^0(\xi',t)|^2}. \quad (4.19)$$

For $\beta < 0$, η_s is governed by

$$\dot{\eta}_s(t) \sim \frac{1}{|A_0(t)|^2}, \quad (4.20)$$

which can be integrated to find

$$\eta_s(t) = \eta_s(t_0) + \int_{t_0}^{t} \frac{dt'}{|A_0(t')|^2}, \quad (4.21)$$

where t_0 is a time where η_s is small enough for the equations to asymptotically hold. Clearly, since A_0 has contributions from every part of the conformal map besides the singularity, there is no reason to expect the singularity to slow down as it approaches the real axis; $\beta < 0$ singularities will hit the real axis in finite time.

For $0 < \beta < \frac{1}{2}$, $\eta_s(t)$ is governed by

$$\frac{\dot{\eta}_s(t)}{[-\eta_s(t)]^{2\beta}} \sim \frac{2}{\pi} \frac{1}{|E_0(t)|^2} \int_0^{\infty} ds(1+s^2)^{\beta-1} \equiv M_1(t). \quad (4.22)$$

We also find, from Eq. (4.17), that

$$\frac{d}{dt}|E_0|^2 \sim 2(1-\beta)[-\eta_s(t)]^{2\beta} \frac{2}{\pi} \int_0^{\infty} ds[(1+s^2)^{\beta-1} \\ -2(1+s^2)^{\beta-2}]. \quad (4.23)$$

Combining Eqs. (4.22) and (4.23), we find for $0 < \beta < \frac{1}{4}$, *not* $0 < \beta < \frac{1}{2}$, as claimed previously [36], that

$$\eta_s(t) \sim \eta_s(t_0)\left(1 - \frac{t}{t_s}\right)^{1/(1-4\beta)}, \quad (4.24)$$

where t_s is the time the singularity hits the real axis. The case $\frac{1}{4} < \beta < \frac{1}{2}$ remains unclear at this time. A tacit assumption in this analysis is that the local behavior in Eq. (4.18) holds all the way to the real axis for sufficiently small η_s. This assumption may be violated if there is an additional singularity at ζ_s^* on some other Riemann sheet, which could happen if β is not an integer.

For $\beta > \frac{1}{2}$, $\eta_s(t)$ is governed by

$$\frac{\dot{\eta}_s(t)}{\eta_s(t)} \sim -\frac{1}{\pi} \int_{-\infty}^{+\infty} \frac{d\xi'}{[\xi' - \xi_s(t)]^2} \frac{1}{|z_\zeta^0(\xi',t)|^2} \equiv -M_2(t), \quad (4.25)$$

where

$$z_\zeta^0 \equiv z_\zeta - E(\zeta,t)(\zeta - \zeta_s)^{-\beta} + E(\zeta,t)(\zeta - \xi_s)^{-\beta} \quad (4.26)$$

is just the conformal map with the singularity ζ_s placed on the real axis. The integral in Eq. (4.25) is not a principal-value integral. In the vicinity of the singularity, the integrand in Eq. (4.25) has the behavior

$$\frac{d\xi'}{[\xi' - \xi_s(t)]^2} \frac{1}{|z_\zeta^0(\xi',t)|^2} \sim d\xi' \frac{|\xi' - \xi_s(t)|^{2(\beta-1)}}{|E_0(t)|^2}. \quad (4.27)$$

We see that if $\beta > \frac{1}{2}$, then the integrand contains at most an integrable singularity, and if $\beta > 1$, then the integrand goes to zero at ξ_s. Therefore, if $\beta > \frac{1}{2}$, then there is no problem in evaluating the integral in Eq. (4.25). Equation (4.25) can be integrated to find

$$\eta_s(t) = \eta_s(t_0)\exp\left(-\int_{t_0}^{t} dt' M_2(t')\right), \quad \beta > \frac{1}{2}. \quad (4.28)$$

We also find, from Eq. (4.17), that

$$E_0(t) \sim E_0(t_0)\left(\frac{\eta_s(t_0)}{\eta_s(t)}\right)^{1-\beta} = K_0[-\eta_s(t)]^{\beta-1}, \quad (4.29)$$

where K_0 is a constant. From Eq. (4.28) we see that a $\beta > \frac{1}{2}$ singularity could only hit the real axis if $M_2(t)$ goes to infinity. Considering the dependence of M_2 on E_0 in Eq. (4.27) and the dependence of E_0 on η_s in Eq. (4.29), we conclude that $\beta > \frac{1}{2}$ singularities slow down as they approach the real axis and do not hit in finite time. More information can be obtained for a $\beta > \frac{1}{2}$ singularity as it asymptotically approaches the ξ axis at long times. We begin by examining the behavior of the real part $\xi_s(t)$. For $t \to \infty$, if $|\xi_s| \to \infty$ also, then Eq. (4.19) tends to

$$\dot{\xi}_s(t) \sim \frac{1}{\pi\xi_s(t)} \int_{-\infty}^{+\infty} \frac{d\xi'}{|z_\zeta^0(\xi',t)|^2}. \quad (4.30)$$

In general, all of the singularities make some contribution to z_ζ^0, not just the particular ζ_s under consideration. However, it can be easily shown that for precisely a single pole ($\beta = 1$), the integral in Eq. (4.30) approaches a constant at long time. Moreover, for an arbitrary initial distribution of singularities, those far from the real axis make negligible contributions to the integral; those that have come close to the axis make $O(|\eta_s|^{2\beta}/|E_0|^2)$ contributions, and from Eq. (4.29), this is found to be small. Utilizing the fact that, at long times, the integral approaches a constant, we obtain from Eq. (4.30)

$$\xi_s^2(t) \sim 2It + C, \quad t \to \infty$$

$$I \equiv \frac{1}{\pi} \int_{-\infty}^{\infty} \frac{d\xi'}{|z_\zeta^0(\xi',t)|^2}, \quad (4.31)$$

where C is a constant of integration, related to the initial location of the singularity.

Obtaining the long-time asymptotic behavior of η_s from Eqs. (4.25) or (4.28) depends on finding the proper long-time asymptotic evaluation of the integral $M_2(t)$, defined in Eq. (4.25). Breaking up the integral in $M_2(t)$ into an inner region adjacent to the singularity and outer regions and then substituting into Eq. (4.25), we find that Eq. (4.25) reduces to

$$\frac{\dot{\eta}_s}{\eta_s} \sim -\frac{I}{\xi_s^2} - \frac{R_0(\beta)}{|K_0|} \frac{\xi_s^{1/\beta-2}}{(-\eta_s)^{1-1/\beta}}, \qquad (4.32)$$

where

$$R_0(\beta)$$

$$\equiv \frac{2}{\pi\beta} \sin\left(\frac{\pi\beta}{2}\right) \cos\left(\phi - \frac{\pi\beta}{2}\right)$$

$$\times \int_0^\infty \frac{u^{2-1/\beta}du}{(u^2 - 2\sin\phi\,u + 1)[u^2 - 2\sin(\phi - \pi\beta)u + 1]}, \qquad (4.33)$$

and $\phi = \arg(E_0) = \arg(K_0)$.

There are three different asymptotically valid limiting forms of Eq. (4.32), depending upon the value of β. First, for the case of a pole ($\beta = 1$), the second term on the right-hand side of Eq. (4.32) is easily seen to be $O(1/\xi_s)$ and so dominates the first term. Interestingly, this means that global effects do not have an impact on the motion of the pole. Integrating, we have

$$\eta_s \sim -C \exp\left(-\frac{1}{\mathrm{Re}(E_0)} \sqrt{\frac{2t}{I}}\right), \quad t \to \infty, \quad \beta = 1. \quad (4.34)$$

However, for $\beta \neq 1$, both terms may be comparable. Proceeding on that basis, the solution is in the form $\eta_s \sim -Ct^{-\gamma}$, $\gamma = 1/[2(1-\beta)]$, and substitution into Eq. (4.32) gives

$$C^{1-1/\beta} = \frac{2(1-\beta)R_0}{|K_0|} (2I)^{(1/2\beta)-1},$$

$$\eta_s \sim -Ct^{-1/[2(1-\beta)]}, \quad t \to \infty, \quad \tfrac{1}{2} < \beta < 1, \quad (4.35)$$

where the obvious requirement that $\beta < 1$ has been appended, since η_s is required to be small in this analysis. In fact, for $\beta > 1$, only the first term of Eq. (4.32) is important, as may be verified *a posteriori* by a substitution of η_s proportional to $t^{-1/2}$ into Eq. (4.32). That results in simply

$$\eta_s \sim -Ct^{-1/2}, \quad t \to \infty, \quad \beta > 1. \qquad (4.36)$$

Hence we see that poles of z_ζ ($\beta = 1$) approach the real axis exponentially fast, but branch point singularities approach algebraically as a power of $1/t$. This means that, at least for $\mathcal{B} = 0$ dynamics, with an initial set of singularities at arbitrary locations, the deformation of the crystal boundary due to poles will dominate the long-time behavior.

Note that on the real axis, the deformation caused by an approaching pole singularity is

$$z_\zeta(\xi_s, t) \sim \frac{E_0(t)}{[-i\eta_s(t)]^\beta} \sim \frac{K_0}{-i\eta_s(t)}$$

$$\sim i\frac{K_0}{C} \exp\left(\frac{1}{\mathrm{Re}(E_0)} \sqrt{\frac{2t}{I}}\right). \qquad (4.37)$$

Since the y location of the disturbance is $-\xi_s^2/2 \sim -It$, it follows that the disturbance grows as

$$z_\zeta(\xi_s, t) \sim i\frac{K_0}{C} \exp\left(\frac{1}{\mathrm{Re}(E_0)} \sqrt{\frac{2|y_s|}{I^2}}\right). \qquad (4.38)$$

An unspoken assumption in Eq. (4.38) is that $\mathrm{Re}(E_0)/\mathrm{Im}(E_0) \neq 0$. We will see in the next section that, at least for poles, this assumption is required in order for $|\xi_s| \to \infty$ as $t \to \infty$. In the context of the $\mathcal{B} = 0$ dynamics, there is no limit how small $|E_0|$ can be, so that Eq. (4.38) allows arbitrarily large growth rates. Ultimately, surface-energy effects set a minimum allowed $|E_0|$, which limits the growth rate of disturbances.

V. A CLASS OF EXACT ZERO-SURFACE-ENERGY SOLUTIONS: INITIAL POLE SINGULARITIES

Although the zero-surface-energy problem formulated in the preceding section is quite general and can be solved numerically by the method of Baker, Siegel, and Tanveer [37] we can obtain many more analytical results if we specialize the initial conditions to include only poles of z_ζ and constant E_j's. Furthermore, solving these specialized equations numerically only requires the integration of ordinary differential equations (similar to Ref. [33]) rather than the integration of the integro-differential equations (4.14) as in the aforementioned paper. We first integrate these ordinary differential equations analytically in a "small-residue" ($E_j \to 0$) limit that is nonlinear at the leading order. We then relate these asymptotic results to the more general $E_j = O(1)$ case and then integrate the system of ordinary differential equations numerically.

If we restrict our attention to initial conditions with all $\beta_j = 1$, the problem simplifies dramatically. The conformal map $z(\zeta, t)$ will contain only logarithmic singularities, so the derivative z_ζ will contain only poles. The integrals depend only on z_ζ, so they can be evaluated exactly with the residue theorem. We begin with the conformal map (4.11)–(4.15) and the governing equations (4.14), specialized to $\beta_j = 1$ and with the $E_j(\zeta, 0) = E_j$ chosen as constant for all j. One can show from Eq. (4.13) that when $\beta = 1$ and E_j is initially independent of ζ, then E_j will remain independent of ζ as well as t for $t > 0$. Without any branch points in their integrands, we can evaluate q_1 [defined in Eq. (4.2)] and $b_0(t)$ [defined in Eq. (4.16)] using the residue theorem. Now all the poles are in the lower-half plane and z_ζ is analytic in the upper-half plane, so all contributions to the integrals come from the residues due to the zeros of $\tilde{z}_\zeta$, which, it turns out, are just the complex conjugates of the zeros of z_ζ. Since the combined numerators of z_ζ form an $(N+1)$st-order polynomial, there are $N+1$ zeros. The integro-differential equations are thus reduced to a system of ordinary differential equations for the pole trajectories

$$z(\zeta,t) = -\frac{i}{2}\,\zeta^2 + \zeta + b_0(t) + \sum_{j=1}^{N} E_j\,\ln[\zeta - \zeta_{sj}(t)], \quad (5.1)$$

$$z_\zeta(\zeta,t) = -i\zeta + 1 + \sum_{j=1}^{N} \frac{E_j}{\zeta - \zeta_{sj}(t)}, \quad (5.2)$$

$$\dot{b}_0(t) = -2\sum_{n=1}^{N+1} \frac{1}{\widetilde{z}_{\zeta\zeta}(\zeta_{0n}^*(t),t)z_\zeta(\zeta_{0n}^*(t),t)}, \quad (5.3)$$

$$\dot{\zeta}_{sj}(t) = -2i\sum_{n=1}^{N+1} \frac{1}{\widetilde{z}_{\zeta\zeta}(\zeta_{0n}^*(t),t)z_\zeta(\zeta_{0n}^*(t),t)[\zeta_{0n}^*(t) - \zeta_{sj}(t)]}, \quad (5.4)$$

$$z_\zeta(\zeta_{0n}(t),t) = 0, \quad n=1,\dots,N+1, \quad (5.5)$$

$$\widetilde{z}_\zeta(\zeta,t) = (z_\zeta(\zeta^*,t))^*. \quad (5.6)$$

This formulated problem for the conformal map evolution is ''exact'' in the sense that no numerical approximation was needed to evaluate the integrals. Similar solutions are reported in the literature for the Hele-Shaw problem [33,44–47].

As in Sec. IV, we can look at the behavior of a pole that is near the real axis. We evaluate Eqs. (4.19) and (4.25) with the residue theorem to obtain

$$\dot{\xi}_{sj}(t) \sim -2i\sum_{i=1}^{N+1} \frac{1}{\widetilde{z}_{\zeta\zeta}(\zeta_{0i}^*(t),t)z_\zeta(\zeta_{0i}^*(t),t)[\zeta_{0i}^*(t) - \xi_{sj}(t)]}, \quad (5.7)$$

$$\frac{\dot{\eta}_{sj}(t)}{\eta_{sj}(t)} \sim -2i\sum_{i=1}^{N+1} \frac{1}{\widetilde{z}_{\zeta\zeta}(\zeta_{0i}^*(t),t)z_\zeta(\zeta_{0i}^*(t),t)[\zeta_{0i}^*(t) - \xi_{sj}(t)]^2}. \quad (5.8)$$

Since the right-hand sides of Eqs. (4.19) and (4.25) are real valued, the sums on the right-hand sides of Eqs. (5.7) and (5.8) must also be real valued, even though the individual terms in the sums are complex. In the presence of computer roundoff error, the real part of Eq. (5.4) reduces naturally to Eq. (5.7), but the imaginary part of Eq. (5.4) becomes severely contaminated by roundoff error as η_s approaches the machine precision. In the numerical solution of the equations, Eq. (5.8) was used to calculate $d\eta_s/dt$ when η_s is small enough.

For the case when a zero is close to the real axis (ζ_{0j}, for example), the equations for the poles (5.4) reduce to

$$\dot{\zeta}_{sn}(t) \sim \frac{1}{\eta_{0j}(t)}\,\frac{1}{|z_{\zeta\zeta}(\xi_{0j}(t),t)|^2[\xi_{0j}(t) - \zeta_{sn}(t)]}. \quad (5.9)$$

We see that if $\eta_{0j}\to 0$, then all the poles will reach infinite velocity, so that a zero impact generates a global effect. The formulated set of Eqs. (5.1)–(5.6) generally requires a numerical solution. However, we look first at the case of small E_j and solve the system of equations in closed form, asymptotically.

A. Small-residue theory

If we now investigate the case where all the pole residues E_j are small, further analytical progress is possible. For arbitrary residues, analytical progress is hampered because the location of the $N+1$ zeros is generally impossible to find analytically. However, if the residues are small, the zeros can be found asymptotically with a regular perturbation series. With the zeros known, we can then integrate the equations asymptotically as well. Once the pole trajectories are known, we can calculate the conformal map from Eq. (5.1) to determine the interface shape. Since the poles will still approach the real axis indefinitely, we are in no way limiting the *small-residue* theory to small *disturbances*; it is a fully nonlinear theory, the only restriction being in the nature of the disturbances.

We now want to make the connection between the initial singularity location and residue and the presence of small initial disturbances in the interface. Equations (4.11) and (5.1) are not limited to small initial noise; they apply equally well to large initial disturbances. From Eq. (5.2), requiring the initial interface disturbances to have small slopes requires

$$\sum_{j=1}^{N} \frac{E_j}{\xi - \zeta_{sj}(0)} = O(\epsilon), \quad (5.10)$$

where ϵ is a measure of the size of the noise or roundoff error at initial time and is *not* related in any way to the ϵ of Sec. III. This ordering is satisfied if

$$\frac{E_j}{-i\,\eta_{sj}(0)} = O(\epsilon) \quad (5.11)$$

for all j. If we now make the further assumption that all $\eta_{sj}(0) = O(1)$, then we arrive at the small-residue problem

$$E_j = \epsilon\hat{E}_j, \quad \eta_{sj}(0) = O(1),$$

$$z(\zeta,t) = -\frac{i}{2}\,\zeta^2 + \zeta + b_0(t) + \epsilon\sum_{j=1}^{N} \hat{E}_j\,\ln[\zeta - \zeta_{sj}(t)],$$

$$z_\zeta(\zeta,t) = -i\zeta + 1 + \epsilon\sum_{j=1}^{N} \frac{\hat{E}_j}{\zeta - \zeta_{sj}(t)}. \quad (5.12)$$

An examination of the conformal map on the crystal-melt interface indicates that small ϵ leads to narrow disturbances in the vicinity of ξ_{sj}, when the pole is close enough to the real (ξ) axis, but that the *depth* of the disturbance depends on ζ_{sj}, which can become anything by an appropriate choice of initial conditions. This implies that the small-residue theory is not a linearized small-disturbance theory, even though the interface disturbances are chosen to be initially small.

With the above form for z_ζ, we can determine the zeros asymptotically from the conformal map. Under some restrictions noted below, the zeros of z_ζ are given by

$$\zeta_{0j} \sim \zeta_{sj} - \epsilon\,\frac{i\hat{E}_j}{i+\zeta_{sj}} + O(\epsilon^2), \quad j=1,\dots,N \quad (5.13)$$

$$\zeta_{0N+1} \sim -i + \epsilon \sum_{n=1}^{N} \frac{i\hat{E}_n}{i+\zeta_{sn}} + O(\epsilon^2), \quad (5.14)$$

$$|\zeta_{sj} - \zeta_{sn}| \gg \epsilon, \quad j \neq n, \quad (5.15)$$

$$|i+\zeta_{sn}| \gg \epsilon. \quad (5.16)$$

In deriving these results, we take the poles as known quantities. We see from Eq. (5.13) that each pole has a companion zero and that the zero's trajectory depends only on its poles to this order. The $(N+1)$st zero (5.14) arises from the underlying Ivantsov solution, the ''Ivantsov zero'' (as it is present in the Ivantsov solution). The requirement that the poles not be too close together (5.15) ensures that the first N zeros are independent of the other poles to this order. The last inequality (5.16) requires that the poles not be too close to the Ivantsov zero (5.14). With this knowledge of the zero locations, it is easy to determine a criterion for cusp formation caused by zeros impacting the real axis in this limit. Since all of the poles are destined to move arbitrarily close to the real axis [by Eq. (4.8)] and their companion zeros are forced to be $O(\epsilon)$ away from the poles [by Eq. (5.13)], cusps will be prevented if $|\eta_{0j}| > |\eta_{sj}|$ as $\eta_{sj} \to 0$ for all j. In terms of the residues, this requirement can be obtained from Eq. (5.13),

$$\text{Re}(E_j)\xi_{sj} + \text{Im}(E_j) > 0 \quad \text{for } |\eta_{sj}(t)| \to 0. \quad (5.17)$$

This requirement will be related to the initial data shortly.

With the zeros known, we now find the singularity trajectories. We begin with the regular perturbation

$$\zeta_{sj}(t) \sim \zeta_{s0j}(t) + \epsilon\zeta_{s1j}(t) + O(\epsilon^2),$$

$$\zeta_{0j}(t) \sim \zeta_{00j}(t) + \epsilon\zeta_{01j}(t) + O(\epsilon^2),$$

$$q_1(\zeta,t) \sim q_{10}(\zeta,t) + \epsilon q_{11}(\zeta,t) + O(\epsilon^2). \quad (5.18)$$

One convenient quantity that will show up repeatedly in the analysis below is

$$\left(\frac{\zeta_{0j} - \zeta_{sj}}{\epsilon}\right) \sim -\frac{i\hat{E}_j}{i+\zeta_{s0j}(t)} = O(1). \quad (5.19)$$

In the perturbation analysis, we find four distinct behaviors and we examine each in turn:

$$(1) \quad \eta_{sj} = O(1), \quad (2) \quad \eta_{sj} = O(\epsilon),$$

$$(3) \quad |\eta_{sj}| \ll \epsilon, \quad \text{and} \quad (4) \quad |\eta_{0j}| \ll \epsilon.$$

1. $\eta_{sj} = O(1)$: Initial trajectories and breakdown of the attempted regular perturbation series

We begin with $\eta_{sj} = O(1)$. The asymptotic terms for q_1 are

$$q_{10}(\zeta_{s0j}(t),t) \equiv [q_1(\zeta_{s0j}(t),t)]_{\epsilon=0}$$

$$= \frac{1}{i-\zeta_{s0j}(t)} = q_{10}(\zeta_{s0j}(t)), \quad (5.20)$$

$$q_{11}(\zeta_{s0j}(t),t) \equiv \left(\frac{\partial q_1(\zeta_{s0j}(t),t)}{\partial\epsilon}\right)_{\epsilon=0}$$

$$= -\left(\frac{\zeta_{0j}^* - \zeta_{sj}^*}{\epsilon}\right)(t)\left(\frac{1}{[\zeta_{s0j}^*(t)]^2 + 1}\right)\frac{1}{\eta_{s0j}(t)}$$

$$+ \hat{q}_{11}(t). \quad (5.21)$$

The form of q_{10} arises from the $(N+1)$st term in q_1. (The Ivantsov-zero effects dominate the effects of the other zeros.) The influence of all the other zeros come in at the q_{11} term, where the first part arises from the jth term in q_1 (due to the pole's companion zero) and $\hat{q}_{11}$ is a messy sum of terms that are all well behaved as $\eta_{sj} \to 0$. The pole-interaction effects are all contained in the $\hat{q}_{11}$ term.

The leading-order behavior is determined by integrating [from Eq. (5.4)]

$$\dot{\zeta}_{s0j} = -q_{10}(\zeta_{s0j}(t),t) = -\frac{1}{i-\zeta_{s0j}},$$

$$\zeta_{s0j}(0) = \zeta_{sj}(0). \quad (5.22)$$

Fortunately, these nonlinear equations for the pole trajectories are easily integrated to get

$$\zeta_{s0j}(t) = i + \sqrt{2t + [\zeta_{sj}(0) - i]^2}, \quad (5.23)$$

where the square-root branch is chosen so that $|\text{Im}(\zeta_{s0j})|$ decreases with time. We make several observations about Eq. (5.23). First, not only are the poles decoupled at leading order, their trajectories are independent of their residues E_j at the leading order too. Second, the imaginary axis acts as a separatrix in that poles in quadrant III move to the left and poles in quadrant IV move to the right. Third, the assumption $|\eta_{sj}| = O(1)$ is violated in $O(1)$ time for each j, so that Eq. (5.23) is the trajectory only initially. With the assistance of Eq. (5.23), we can now construct initial conditions that avoid cusps. Define

$$\zeta_{s0j}(t_1) \equiv \xi_{s0j}(t_1) = i + \sqrt{2t_1 + [\zeta_{sj}(0) - i]^2}$$

$$\Rightarrow \xi_{s0j}(t_1) = \xi_{sj}(0)[1 - \eta_{sj}(0)]$$

$$\Rightarrow t_1 = \frac{1}{2}\{[1 - \eta_{sj}(0)]^2 - 1\}[\xi_{sj}^2(0) + 1]. \quad (5.24)$$

We then combine Eq. (5.24) with Eq. (5.17) to find that cusps are prevented if

$$\text{Re}(E_j)\xi_{sj}(0)[1 - \eta_{sj}(0)] + \text{Im}(E_j) > 0. \quad (5.25)$$

This is, of course, an asymptotic cusp prevention criterion that is not exact, but valid in the $\epsilon \to 0$ limit. Inequality (5.25) provides the cusp-prevention criterion in terms of the initial data. If we deliberately violate Eq. (5.25), then a cusp will form at $t \sim t_1$ and $z \sim z(\xi_{s0j}(t_1), t_1)$, as defined in Eq. (5.24).

From Eq. (5.13), we know that the zeros and poles are at the same location to leading order, so we need to find ζ_{s1} to distinguish the pole trajectories from the zero trajectories. The governing equation is

$$\zeta_{s1j}(t) = -q_{10\zeta}(\zeta_{s0j}(t))\zeta_{s1j}(t) - q_{11}(\zeta_{s0j}(t),t),$$

$$\zeta_{s1j}(0) = 0, \tag{5.26}$$

which is a linear, first-order ordinary differential equation that has the solution

$$\zeta_{s1j}(t) = -q_{10}(\zeta_{s0j}(t)) \int_0^t dt' \, \frac{q_{11}(\zeta_{s0j}(t'),t')}{q_{10}(\zeta_{s0j}(t'))}. \tag{5.27}$$

We know from Eqs. (5.21) and (5.24) that the integrand in Eq. (5.27) is singular as $t \to t_1$. If we add and subtract the form of the singularity in the integrand of Eq. (5.27) and then perform the integration, we find that ζ_{s1} has the form

$$\zeta_{s1j}(t) = \left(\frac{i - \xi_{s0j}(t_1)}{i - \zeta_{s0j}(t)} \right) \left(\frac{\zeta_{0j}^* - \zeta_{sj}^*}{\epsilon} \right)(t_1)\ln(t_1 - t) + \hat{\zeta}_{s1j}(t), \tag{5.28}$$

where $\hat{\zeta}_{s1j}$ is the contribution that is well behaved at $t = t_1$. This solution (5.28) is still an exact representation for ζ_{s1}. The presence of the logarithm indicates that the solution breaks down as the pole nears the real axis. In the neighborhood of $t = t_1$, the outer solution becomes

$$\zeta_{sj}(t) \sim \xi_{s0j}(t_1) + \left(\frac{\xi_{s0j}(t_1) + i}{\xi_{s0j}^2(t_1) + 1} \right)(t - t_1)$$

$$+ \epsilon \left(\frac{\zeta_{0j}^* - \zeta_{sj}^*}{\epsilon} \right)(t_1)\ln(t_1 - t) + \epsilon\hat{\zeta}_{s1j}(t). \tag{5.29}$$

We will use this equation in the matching to the $O(\epsilon)$ solution below.

2. $\eta_{sj} = O(\epsilon)$: Inner layer, fast time scale

We now investigate the behavior of the pole in the ϵ layer adjacent to the real axis, $\eta_{sj} = O(\epsilon)$. Define the inner variables

$$t - t_2 = \epsilon\tau,$$

$$\zeta_{sj}(t) - \xi_{s0j}(t_2) = \epsilon\chi_s(\tau),$$

$$t_2 \equiv t_1 + \mu(\epsilon)\tau_1,$$

$$\xi_{s0j}(t_2) \equiv \xi_{s0j}(t_1) + \mu(\epsilon)\text{Re}(E_j),$$

$$\mu(\epsilon) = -\epsilon \ln\epsilon,$$

$$\tau_1 = \text{Re}(\hat{E}_j)\xi_{s0j}(t_1) + \text{Im}(\hat{E}_j). \tag{5.30}$$

Using these inner variables, we obtain the inner equation for χ_s,

$$\dot{\chi}_s(\tau) \sim \left(\frac{\xi_{s0j}(t_2) + i}{\xi_{s0j}^2(t_2) + 1} \right) + \left(\frac{\zeta_{0j}^* - \zeta_{sj}^*}{\epsilon} \right)(t_2) \frac{1}{\xi_{s0j}^2(t_2) + 1}$$

$$\times \frac{1}{\text{Im}[\chi_s(\tau)] + \left(\dfrac{\eta_{0j} - \eta_{sj}}{\epsilon} \right)(t_2)}. \tag{5.31}$$

The solution for χ_s is obtained by separating the real and imaginary parts of Eq. (5.31), integrating the imaginary part, and then using that solution to integrate the real part. The real and imaginary parts thus found are then recombined to obtain an implicit solution for χ_s. The matching to the earlier time solution (5.29) is effected in an intermediate matching zone, as is often the case with matching involving logarithmic terms. The implicit solution for χ_s is

$$\chi_s(\tau) - \left(\frac{\zeta_{0j}^* - \zeta_{sj}^*}{\epsilon} \right)(t_2)\ln\{-[\xi_{s0j}^2(t_2) + 1]\text{Im}[\chi_s(\tau)]\}$$

$$- \hat{\zeta}_{s1j}(t_2) = \left(\frac{\xi_{s0j}(t_2) + i}{\xi_{s0j}^2(t_2) + 1} \right)\tau. \tag{5.32}$$

There are two possibilities to consider next. Either the pole's companion zero hits the real axis or it does not. The case where the zero remains safely away from the real axis is the easier case, so we consider it first.

3. $|\eta_{sj}| \ll \epsilon$: Evolution on an $O(1)$ time scale regained

Since Eq. (5.32) is an implicit solution, it is difficult to picture the pole trajectory in the ϵ layer, but the implicit solution becomes explicit as $\tau \to \infty$. From Eq. (5.32), we observe that as $\tau \to \infty$, $\chi_s(\tau)$ has the behavior

$$\text{Im}[\chi_s(\tau)] \sim - \frac{1}{\xi_{s0j}^2(t_2) + 1} \exp\left(-\frac{\tau}{\tau_2} \right),$$

$$\text{Re}[\chi_s(\tau)] \sim \left(\frac{\text{Re}(\hat{E}_j)}{\text{Re}(\hat{E}_j)\xi_{s0j}(t_2) + \text{Im}(\hat{E}_j)} \right)\tau, \tag{5.33}$$

where

$$\tau_2 = \text{Re}(\hat{E}_j)\xi_{s0j}(t_2) + \text{Im}(\hat{E}_j)$$

$$= -[\xi_{s0j}^2(t_2) + 1]\left(\frac{\eta_{0j} - \eta_{sj}}{\epsilon} \right)(t_1). \tag{5.34}$$

From this definition of τ_2, Eqs. (5.33) have the correct behavior (pole moves closer to the real axis) only if the pole is closer to the real axis than the zero. So, if a cusp was going to form, then Eq. (5.33) is not the correct behavior for the pole. Now the act of letting $\tau \to \infty$ means that we are leaving the $O(\epsilon)$ time scale and returning to an $O(1)$ time scale. We consider the time scale to be $O(1)$ again when $\epsilon \, \text{Im}[\chi_s(\tau)] = \eta_{sj}(t) \ll O(\epsilon)$. In this case, we can finally use the asymptotic equations (5.7) and (5.8) that apply when a pole is sufficiently close to the real axis. If we expand Eqs. (5.7) and (5.8) in the small-residue limit, we find that the governing equations are (now with all the ϵ's absorbed into the E_j's)

$$\dot{\xi}_{sj} \sim \frac{\text{Re}(E_j)}{\text{Re}(E_j)\xi_{sj} + \text{Im}(E_j)}, \tag{5.35a}$$

$$\frac{\dot{\eta}_{sj}}{\eta_{sj}} \sim \frac{-1}{\text{Re}(E_j)\xi_{sj} + \text{Im}(E_j)} \sim -\frac{\dot{\xi}_{sj}}{\text{Re}(E_j)}. \tag{5.35b}$$

From Eq. (5.17) we know that $\text{Re}(E_j)\xi_{sj} + \text{Im}(E_j) > 0$, or else the pole's companion zero ζ_{0j} would have hit the real axis

back when $\eta_{sj}=O(\epsilon)$. Therefore, the ξ direction the pole moves in is determined by the sign of $\text{Re}(E_j)$. The matching conditions are, rewriting Eq. (5.33) in the outer variables,

$$\eta_{sj}(t)\sim -\frac{\epsilon}{\xi^2_{s0j}(t_2)+1}\exp\left(-\frac{t-t_2}{\epsilon\tau_2}\right), \quad (5.36a)$$

$$\xi_{sj}(t)\sim \xi_{sj}(t_2)\left(\frac{\text{Re}(E_j)}{\text{Re}(E_j)\xi_{sj}+\text{Im}(E_j)}\right)(t-t_2). \quad (5.36b)$$

By combining Eq. (5.36b) with Eq. (5.35a), we see that the matching condition for ξ_{sj} is just a Taylor-series expansion about $t=t_2$ so that matching will be automatic. Equations (5.35) can be integrated to find

$$\xi_{sj}(t)\sim -\frac{\text{Im}(E_j)}{\text{Re}(E_j)}+\text{sgn}[\text{Re}(E_j)]$$
$$\times \sqrt{2(t-t_2)+\left(\xi_{s0j}(t_2)+\frac{\text{Im}(E_j)}{\text{Re}(E_j)}\right)^2},$$

$$\eta_{sj}(t)\sim -\frac{\epsilon}{\xi^2_{s0j}(t_2)+1}\exp\left(\frac{\xi_{s0j}(t_2)-\xi_{sj}(t)}{\text{Re}(E_j)}\right) \quad (5.37)$$

if $\text{Re}(E_j)\neq 0$ and

$$\xi_{sj}(t)\sim \xi_{s0j}(t_2),$$

$$\eta_{sj}(t)\sim -\frac{\epsilon}{\xi^2_{s0j}(t_2)+1}\exp\left(\frac{t-t_2}{\text{Im}(E_j)}\right) \quad (5.38)$$

if $\text{Re}(E_j)=0$. Equations (5.37) are actually uniformly valid as $\text{Re}(E_j)/\text{Im}(E_j)\to 0$, with Eq. (5.38) as the limiting form.

With these results (5.37), we can say something about the behavior of the singularities as they move very close to the real axis. First, we see that the pole approaches the real axis exponentially fast and moves along the real axis like $\sqrt{t}$ [cf. Eq. (4.31)]. Now let us say, for example, that $\xi_{sj}(t_2)>0$. If $\text{Re}(E_j)>0$, then the pole will continue to move toward $\xi=+\infty$ without further incident, at least until surface-energy effects become important. On the other hand, if $\text{Re}(E_j)<0$, then the pole will be heading toward $\xi=-\infty$, but along the way it will have to cross the imaginary axis. When the pole crosses the imaginary axis, the corresponding indentation in the crystal-melt interface will cross the tip; a tip splitting will occur. Tip splitting is prevented in these solutions if

$$\text{sgn}[\text{Re}(E_j)]=\text{sgn}[\xi_{sj}(0)], \quad (5.39)$$

so that the pole does not change quadrants. Finally, the pole creates an indentation in the crystal-melt interface (at a fixed location in the laboratory frame [37]), oriented at an angle

$$\theta_{\text{indent}}=\tan^{-1}\left(-\frac{\text{Re}(E_j)}{\text{Im}(E_j)}\right) \quad (5.40)$$

with respect to the y axis. Since the E_j's are specified quantities, the angles of the indentations are fully determined by the initial conditions we specify; we have full control to make them whatever we want them to be. Random initial conditions would therefore have a random distribution of indentation angles in this zero-surface-energy case.

4. $|\eta_{0j}|\ll\epsilon$: Imminent cusp formation and global effects

If the pole's companion zero is going to hit the real axis, it will occur while the pole is in the ϵ layer. In terms of the inner variables, the zero's location is given by

$$\zeta_{0j}\sim \xi_{s0j}(t_2)+\epsilon\chi_s(\tau)+\epsilon\left(\frac{\zeta_{0j}-\zeta_{sj}}{\epsilon}\right)(t_2),$$

$$\text{Im}[\chi_0(\tau)]\sim \text{Im}[\chi_s(\tau)]+\left(\frac{\eta_{0j}-\eta_{sj}}{\epsilon}\right)(t_2). \quad (5.41)$$

The implicit equation for the zero is obtained by combining Eqs. (5.41) and (5.32). We only look at the imaginary part here,

$$\text{Im}[\chi_0(\tau)]+\left(\frac{\eta_{0j}-\eta_{sj}}{\epsilon}\right)(t_2)\left(\ln\left\{[\xi^2_{s0j}(t_2)+1]\left[\left(\frac{\eta_{0j}-\eta_{sj}}{\epsilon}\right)\right.\right.\right.$$
$$\left.\left.\left.\times(t_2)-\text{Im}[\chi_0(\tau)]\right]\right\}-1\right)-\hat{\eta}_{s1j}(t_2)=\frac{\tau}{\xi^2_{s0j}(t_2)+1}. \quad (5.42)$$

From Eq. (5.42) we find that cusp formation is imminent at

$$\tau_c=-\tau_2[\ln(-\tau_2)-1]-[\xi^2_{s0j}(t_2)+1]\hat{\eta}_{s1j}(t_2). \quad (5.43)$$

Using Eq. (5.43), we can write the imaginary part of the zero's trajectory as

$$\text{Im}[\chi_0(\tau)]+\left(\frac{\eta_{0j}-\eta_{sj}}{\epsilon}\right)(t_2)\ln\left[1-\frac{\text{Im}[\chi_0(\tau)]}{\left(\frac{\eta_{0j}-\eta_{sj}}{\epsilon}\right)(t_2)}\right]$$

$$=\frac{\tau-\tau_c}{\xi^2_{s0j}(t_2)+1}. \quad (5.44)$$

In the limit of $\tau\to\tau_c$, Eq. (5.44) can be solved for $\text{Im}(\chi_0)$,

$$\text{Im}[\chi_0(\tau)]\sim -\left[\frac{2}{\xi^2_{s0j}(t_2)+1}\left(\frac{\eta_{0j}-\eta_{sj}}{\epsilon}\right)(t_2)(\tau_c-\tau)\right]^{1/2}. \quad (5.45)$$

A zero hitting the real axis, therefore, generates a square-root singularity in finite time and generates a cusp in the interface. We cannot get past the cusp formation without including surface-energy effects.

When cusp formation is imminent, we know from Eq. (5.9) that there is a global effect on the other poles, not just the zero's companion pole. Let us investigate this now. An expansion of the governing equations with $\eta_{0j}\ll O(\epsilon)$ produces

$$\dot{\zeta}_{sk}\sim -\frac{1}{i-\zeta_{sk}}+\frac{|\hat{E}_j|^2}{\left(\frac{\eta_{0j}}{\epsilon^2}\right)[\xi^2_{s0j}(t_2)+1]^2[\xi_{s0j}(t_2)-\zeta_{sk}]}. \quad (5.46)$$

We see that the zero's global effects become leading order when $\eta_{0j}=O(\epsilon^2)$. If we define the inner variables

$$t - t_c = \epsilon^3 \hat{\tau}, \quad \zeta_{sk}(t) - \zeta_{s0k}(t_c) = \epsilon^3 \hat{\chi}_s(\hat{\tau}), \quad t_c = t_2 + \epsilon \tau_c, \quad \zeta_{s0k}(t_c) = i + \sqrt{2t_c + [\zeta_{sk}(0) - i]^2}, \tag{5.47}$$

we find the solution (written in the outer variables again)

$$\zeta_{sk}(t) = \zeta_{s0k}(t_c) - \frac{t - t_c}{i - \zeta_{s0k}(t)} + \epsilon^{3/2} \frac{2|\hat{E}_j|^2 (t_c - t)^{1/2}}{\left[2[\xi_{s0j}^2(t_2) + 1]^3 \left(\dfrac{\eta_{0j} - \eta_{sj}}{\epsilon} \right)(t_2) \right]^{1/2} [\xi_{s0j}(t_2) - \zeta_{s0k}(t_c)]}. \tag{5.48}$$

We see from Eq. (5.48) that, although the zero had a global influence on the poles, there just was not enough time left before cusp formation to deflect the pole trajectories significantly.

B. Connection between $E_j = O(\epsilon)$ and $O(1)$ theories

After having found a lot of nice analytical results for the $E_j = O(\epsilon)$ case, we would like to try to generalize the results to larger E_j's. Consider the assumptions made above so that the small-residue theory holds,

$$E_j = O(\epsilon), \quad |\zeta_{si} - \zeta_{sj}| \gg \epsilon,$$

$$|i + \zeta_{sj}| \gg \epsilon, \quad -\eta_{sj}(0) \gg \epsilon. \tag{5.49}$$

The result of these assumptions is that the singularity trajectories display four types of behavior

$$-\eta_{sj}(t) \gg \epsilon \Rightarrow \text{Eqs. (5.23) and (5.28)},$$

$$-\eta_{sj}(t) = O(\epsilon) \Rightarrow \text{Eq. (5.32)},$$

$$-\eta_{sj}(t) \ll \epsilon \Rightarrow \text{Eqs. (5.37) and (5.38)},$$

$$-\eta_{0j}(t) \ll \epsilon \Rightarrow \text{Eqs. (5.45) and (5.48)}. \tag{5.50}$$

Now consider the following generalization of assumptions (5.49):

$$E_j = O(\epsilon^\lambda), \quad 0 < \lambda \leqslant 1,$$

$$|\zeta_{si} - \zeta_{sj}| \gg \epsilon^\lambda, \quad |i + \zeta_{sj}| \gg \epsilon^\lambda, \quad -\eta_{sj}(0) \gg \epsilon^\lambda. \tag{5.51}$$

The basic change in the assumptions is that if the pole residues are larger, then the poles must be further apart, further from the Ivantsov zero, and initially further from the real axis. Under these modified assumptions, the different orders of η_{sj} become

$$-\eta_{sj}(t) \gg \epsilon^\lambda, \quad -\eta_{sj}(t) = O(\epsilon^\lambda),$$

$$-\eta_{sj}(t) \ll \epsilon^\lambda, \quad -\eta_{0j}(t) \ll \epsilon^\lambda. \tag{5.52}$$

The results of the new theory are virtually the same; we just replace ϵ with ϵ^λ.

Now consider the limit as $\lambda \to 0$,

$$E_j = O(1), \quad |\zeta_{si} - \zeta_{sj}| \gg 1,$$

$$|i + \zeta_{sj}| \gg 1, \quad --\eta_{sj}(0) \gg 1. \tag{5.53}$$

The third assumption means that the poles are far from the Ivantsov zero and hence far from the origin. This implies that the generalization of the small-residue theory holds if the singularities are far apart and far along the sides of the crystal (but still in region I, of course). Now the orders become

$$-\eta_{sj}(t) \gg 1, \quad -\eta_{sj}(t) = O(1),$$

$$-\eta_{sj}(t) \ll 1, \quad -\eta_{0j}(t) \ll 1. \tag{5.54}$$

The last assumption in Eq. (5.53) states that we start far enough from the real axis that Eq. (5.23) will be the initial trajectory. We do not really have to satisfy this assumption (unless we want the initial interface disturbances to have small slopes). We can start the pole at any distance from the real axis and then investigate the trajectory starting in the appropriate region according to Eq. (5.54). These ordering arguments show that there is a direct correspondence between the small residue theory and a large-ζ_s theory with $O(1)$ residues and well-separated singularities. We do not pursue the details of the connection further since it would be a repetition of Sec. V A.

C. Numerical solutions

We now want to solve the governing equations (5.1) and (5.6) numerically to confirm the small-ϵ theory and so that we are not limited by its assumptions that lead to no-pole interactions. To solve the system of ordinary differential equations, we wrote a complex variable Bulirsch-Stoer equation solver [48,49] complete with variable step size and order control to keep the temporal error within user-specified error tolerances. In spite of the automatic error control, we found that as $\eta_s \to 0$, the error in η_s was not always adequately maintained, so we also included a maximum step size $\Delta t_{\max} = \min|E_j|$ as necessary once the singularities got close to the real axis, in accordance with the small-ϵ time scales found above. The algebraic equations for the zeros (5.5) were solved using Newton's method with the small-ϵ approximations (5.13) and (5.14), with $\epsilon = 1$, providing the initial guess. If the Newton iteration diverges or the calculated zeros are not all distinct, then we explicitly introduce ϵ as a continuation parameter so that the iterations converge and all the zeros are found. As stated previously, the real part of Eq. (5.4) reduces naturally to the asymptotic equation (5.7) in the presence of roundoff error as $\eta_{sj} \to 0$, but the imaginary part becomes severely contaminated by roundoff error. Therefore, we replace the imaginary part of Eq. (5.4) with asymptotic result (5.8) when $|\eta_s| < 10^{-12}$, which worked quite well [50].

We first sought to compare the numerical results to the asymptotic results determined above, both as a test of the
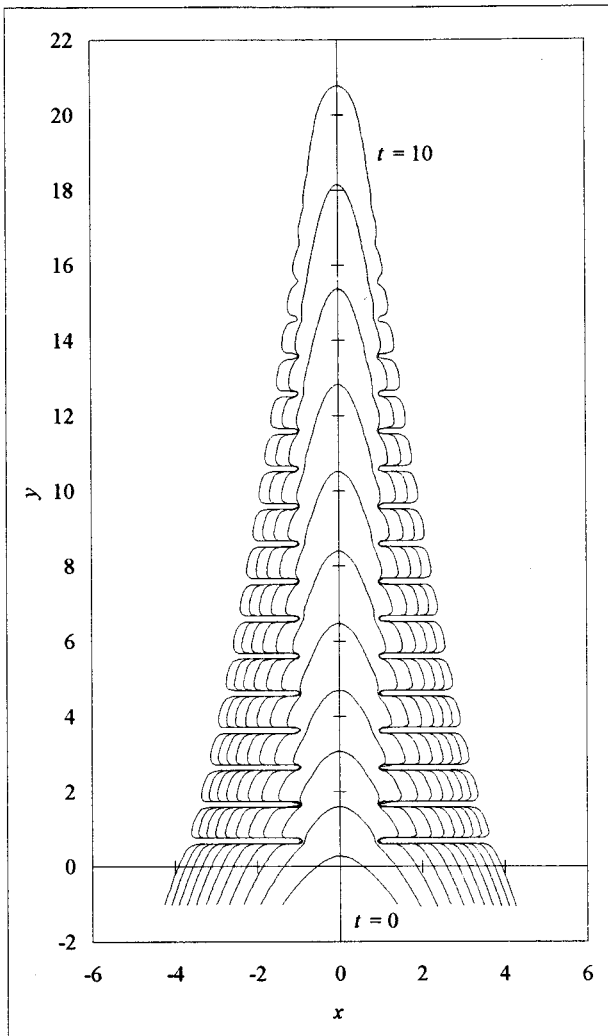
FIG. 5. Forty-pole numerical simulation displaying dendritic behavior.

numerical code and to verify the difficult-to-obtain asymptotic results. This comparison is carried out in great detail by Kunka [50] and the agreement between the numerical results and the theory is outstanding.

We then investigated the effects of many poles on the interface evolution. Ideally, we would use random initial distributions of poles and perform some statistical analysis on the resulting dendrite features. However, we are going to limit our attention here to just a few examples that are not random initial distributions, just to provide some examples of possible interface behavior. Figure 5 shows the dendritic result of a 40-pole simulation from $t=0$ to 10. The initial conditions were chosen with the help of the outer asymptotic behavior (5.23)

$$E_j = \pm 0.05, \quad t_{1j} = j, \quad \xi_{s0j}(t_{1j}) = \pm 1,$$

$$\zeta_{sj}(0) = i \pm \sqrt{[\xi_{s0j}(t_{1j}) - i]^2 - 2t_{1j}}, \quad (5.55)$$

where the "$\pm$" indicates that half the poles are to the right of the imaginary axis and the other half are to the left. We have deliberately chosen initial conditions that will produce a symmetric solution, but nonsymmetric solutions can be

easily generated as well. As time progresses, the poles will approach the real axis in pairs, creating pairs of indentations in the crystal-melt interface. Conditions (5.25) and (5.39) are satisfied, so there will be no cusp formation or tip splitting. Equation (5.40) indicates that the indentations will all be perpendicular to the y axis, the axis of growth. We see for this particular initial condition that the evolving crystal tip is a smooth parabola, which, by the way, is moving about twice as fast as the underlying Ivantsov solution. This speedup is due to the strength of the pole residues E_j and the distance the poles are from the origin when the poles get close to the real axis at $\zeta_{sj} \sim \xi_{sj}(t_1)$. A short distance behind the tip, we see small disturbances in the interface from the poles that are not too close to the interface at this time. Further from the tip, we see deeper indentations due to the poles that are quite close to the real axis. For this particular initial condition, the indentations are all equally spaced and of equal width; this does not happen for random initial conditions. Furthermore, putting indentations next to each other creates growing side branches between them as the indentations grow deeper and deeper. Notice that although the singularities are moving in the ζ plane, the indentations are growing at fixed locations in the z plane. The base of the indentation is also a fixed distance from the y-axis. This distance depends on $\xi_{sj}(t_1)$. Finally, the width of the indentation depends on $|E_j|$; the larger the $|E_j|$, the wider the indentation.

The next generic behavior of the zero-surface energy solutions is tip splitting, obtained when Eq. (5.39) is violated. This time we use the following initial conditions for a one-pole simulation that demonstrates tip splitting:

$$E_j = 0.05(-1+2i),$$

$$t_1 = 1,$$

$$\xi_{20j}(t_1) = 1,$$

$$\zeta_{sj}(0) = i + \sqrt{[\xi_{s0j}(t_1) - i]^2 - 2t_1}. \quad (5.56)$$

The significant difference between this initial condition and initial condition (5.55) is that Eq. (5.39) is violated and E_j now has an imaginary part large enough that Eq. (5.25) is satisfied, so that a cusp does not form. Figure 6 shows the results from $t=0$ to 5. At $t=0$, the pole is far enough from the real axis that the initial interface shape is nearly parabolic. At $t=1$, the pole is close enough to create a sizable disturbance. At $t=2$, the disturbance is deeper and a finger is well developed. Note that the angle of the indentation is across the axis of the crystal, in accordance with Eq. (5.40) and that the location of the opening of the indentation is an indication of the pole's location near the real axis in the ζ plane. At $t=2$, the pole is a little to the right of the imaginary axis in the ζ plane. At $t=3$, the pole is a little to the left of the imaginary axis. As time progresses, the original crystal tip is pushed to the side as the finger in the $t=2$ curve becomes the new crystal tip.

The third generic behavior of the zero-surface-energy solutions is cusp formation, when a zero hits the real axis in the ζ plane. This time, we violate Eq. (5.25) and use the following initial conditions for a one-pole simulation:
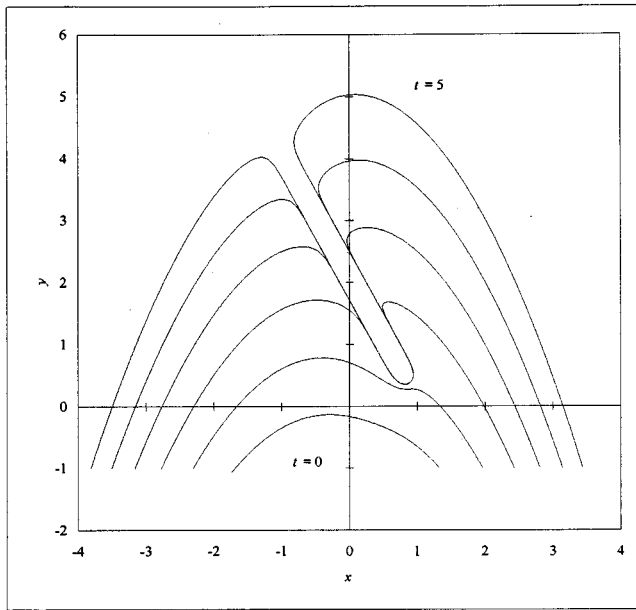
FIG. 6. One-pole simulation displaying tip splitting and competition.

$$E_j = -0.05, \quad t_1 = 1, \quad \xi_{s0j}(t_1) = 1,$$

$$\zeta_{sj}(0) = i + \sqrt{[\xi_{s0j}(t_1) - i]^2 - 2t_1}. \qquad (5.57)$$

Figure 7 shows the interface evolution from $t = 0$ to 0.823 63, where cusp formation occurs. The step-size control in the numerical method signals the onset of cusp formation when the step size rapidly goes to zero. For $t = 0$, 0.2, …, 0.6, the zero (and pole) are far enough from the real axis that the crystal shows nearly steady behavior. Then,
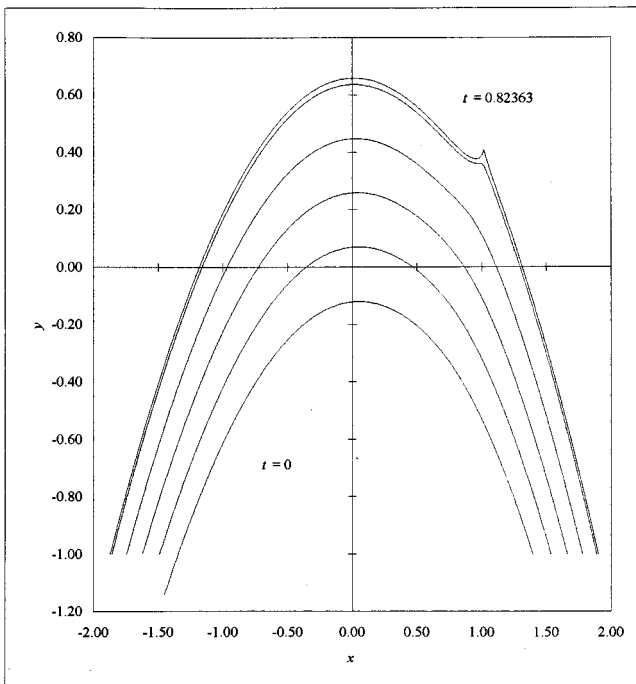
FIG. 7. One-pole simulation at $t = 0, 0.1, …, 0.8, 0.82363$ displaying cusp formation.

at $t = 0.8$, the zero has moved close enough to the real axis to create a bulge that develops into a cusp by $t = 0.823\,63$. When cusps form, the zero-surface-energy solution cannot continue and the numerical solution cannot continue either. This breakdown in the-zero-surface-energy solution indicates that surface energy must become important. Indeed, in certain cases, surface energy effects can become important even when the zero-surface-energy solution corresponds to a smooth interface [36]. We investigate the effects of surface energy on the interface evolution in subsequent parts.

D. Scenario for coarsening

By qualitatively comparing our numerical solutions with the numerous experimental pictures of growing dendrites (such as that of Huang and Glicksman [8]), even though the experiments are three dimensional, we have developed a scenario for coarsening. We caution that this is a "scenario" and not an explanation, as surface energy effects are absent at this time and we expect that only very specific $\mathcal{B} = 0$ solutions are the limiting solutions for $\mathcal{B} \rightarrow 0$. First, recall from Fig. 5 that the poles in the theory create parallel-sided indentations in the crystal-melt interface and that side branches are formed as the interface grows between these indentations. The theory also shows that, since poles approach the real axis exponentially fast [by Eqs. (4.34) and (5.37)], the interface will be most often deformed by pole-type indentations with parallel sides. The experimental pictures confirm this part of the theory; many of the indentations between the sidebranches do seem to have parallel sides.

With the theory suggesting that we look not at the sidebranches but instead at the indentations, we find that there are narrow indentations near the axis of the experimental dendrite with wider indentations further from the central axis. Also the narrower indentations are also found close to the crystal tip, whereas the wider indentations are always much further from the tip. These wider indentations stop the growth of the side branches growing between the narrower indentations.

Figure 8 shows a typical coarsened side-branch structure and the singularity distribution that could generate such a structure. The narrowest indentations that are closest to the crystal core are created by small-E poles that are close to the $\text{Re}(\zeta)$ axis. These poles are also closely spaced, so that the sidebranches are also narrow close to the crystal core. Behind these small-E poles are medium-E poles that create wider indentations and are also spaced further apart, so that the side branch between them is also wider. The presence of these two poles essentially stops the further growth of the smaller side branches. Behind the medium-E poles is a large-E pole that creates the largest indentation at the top of the interface structure. This pole also stops the growth of the side branches formed between the medium-E poles. In the experiments, the large-E poles are also spaced even further apart, so that the growing side branches continue to get wider as they grow further from the central core.

To understand how coarsening occurs, we take this fixed-time singularity distribution based on Fig. 8 and move the singularity distribution back in time to follow the chain of events that leads to the coarsened dendrite. Figure 9 follows the hypothetical trajectories of the small-, medium-, and
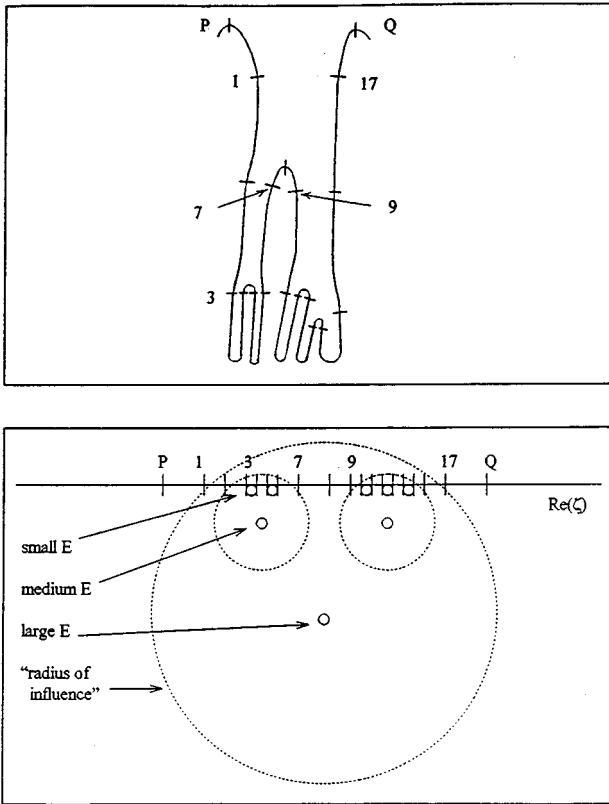
FIG. 8. Interfacial indentations between side branches P and Q and the pole distribution that creates them.

large-E poles used to create a coarsened dendrite such as Fig. 8: At initial time, the small-E poles are relatively close to the Im(ζ) axis, whereas the larger-E poles are further from both the Im(ζ) and the Re(ζ) axes. This initial distribution of singularities is consistent with an initial interface shape that is nearly Ivantsov. As the singularity distribution evolves, a stream of closely spaced, small-E poles comes close to the
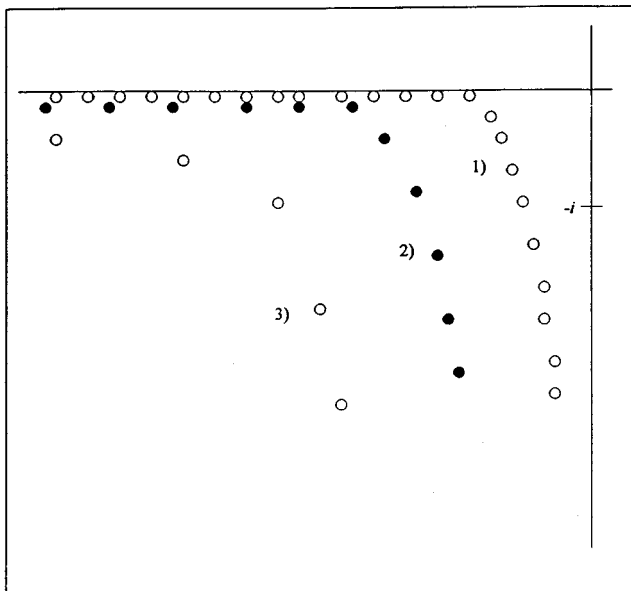
FIG. 9. Singularity distribution that leads to coarsened dendrites: 1, small-E poles; 2, medium-E poles; 3, large-E poles.
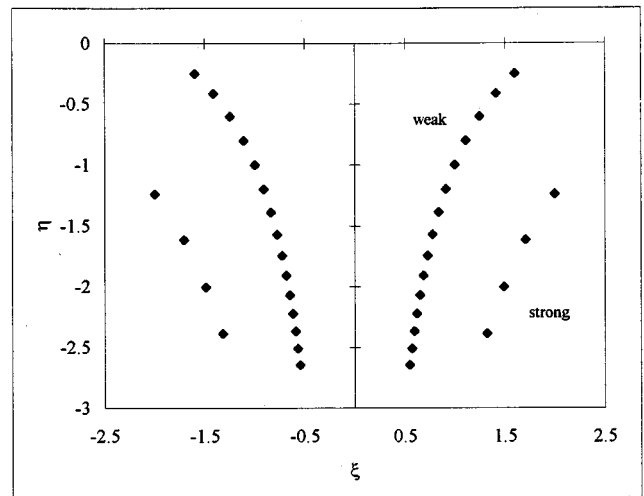
FIG. 10. Initial conditions for coarsened dendrite simulation.

Re(ζ) axis on each side of the crystal at some distance behind the crystal tip. The small-E poles all create narrow indentations that are a fixed distance from the long axis of the dendrite and open away from the long axis, creating the central core of the crystal (as in the numerical solution Fig. 5 above). Later, the medium-E poles come in behind the small-E poles, creating wider indentations and starting the coarsening process. The medium-E poles are spaced further apart and start further from the origin, so that coarsening begins after the initial sidebranches have formed and the active side branches grow wider as they grow longer. Third, the large-E poles come in behind the medium-E poles, creating even wider indentations and thus more coarsening. The large-E poles are spaced even further apart and start further from the origin, so that this stage of the coarsening occurs even further from the crystal tip. The process continues *ad nauseum* as stronger and stronger poles continue to come close to the real axis further and further from the crystal tip.

To add some numerical support for this scenario, we consider the evolution of the initial conditions (Fig. 10)

$$E_{j \text{ weak}} = \pm 0.05, \quad E_{j \text{ strong}} = \pm 0.125,$$

$$t_{1j \text{ weak}} = (j+1)/2, \quad t_{1j \text{ strong}} = 1.45j + 8.55,$$

$$\xi_{s0j}(t_{1j})_{\text{weak}} = \pm 2, \quad \xi_{s0j}(t_{1j})_{\text{strong}} = \pm 4.47,$$

$$\zeta_{sj}(0) = i \pm \sqrt{[\xi_{s0j}(t_{1j}) - i]^2 - 2t_{1j}}. \tag{5.58}$$

We see that the weaker poles are closer to the imaginary axis and that the stronger poles are further from the imaginary axis and further from the real axis so that the initial interface disturbances are not too large. (As a practical matter, we could not make the initial disturbances very small, but this in not important in what develops below).

We first examine the evolution of just the weak singularities (Fig. 11). We deliberately chose the initial conditions so that the poles would create a sequence of narrow indentations that are closely spaced so that the side branches are also narrow.

Now consider the evolution and interaction of both the weak and strong poles (Fig. 12). We make two observations.
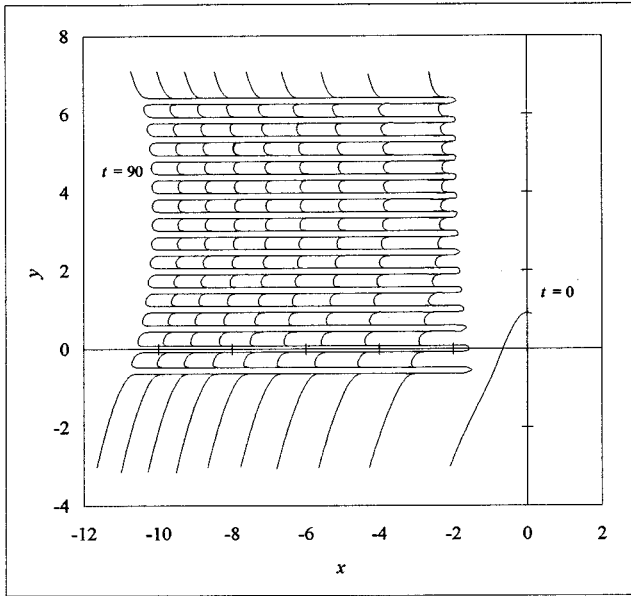
FIG. 11. Simulation with weak poles only.

First, the wider indentations created by the stronger poles *do* stop the growth of the affected side branches. Second, the narrow and wide indentations can interfere and generate nearly cusps and nearly corners. The extreme curvature of the nearly cusp, especially, indicates that surface-energy effects must become important once the zero-surface-energy coarsening has begun. This solution also indicates that the type of evolution arising from more-random initial conditions, which would lead to coarsening somewhere, causes the zero-surface-energy solution ($\mathcal{B}=0$) to deviate from the asymptotic $\mathcal{B}\rightarrow 0$ solution in $O(1)$ time. Contrast this with the solution in Fig. 11, where the lack of interfering indentations causes local surface energy effects to be delayed until $t \gg 1$. We plan to explore these surface-energy effects further in the companion papers.
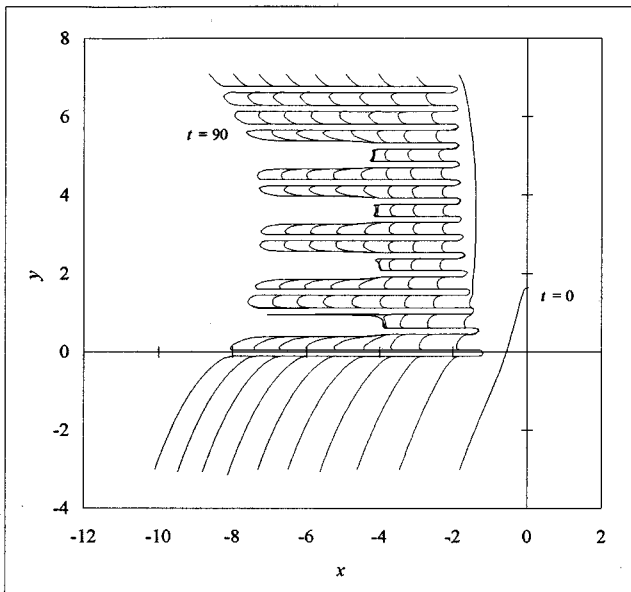

FIG. 12. Simulation with weak and strong poles, displaying coarsening.
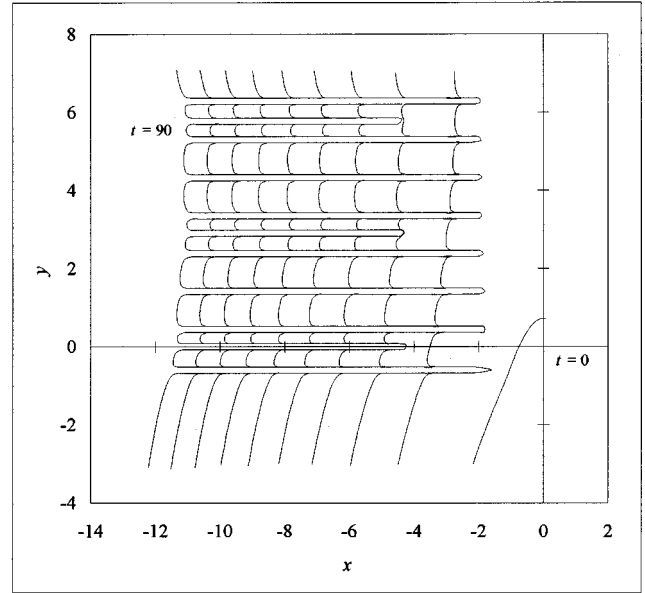
FIG. 13. Simulation with two waves of weak poles, displaying doublon formation.

In addition to a coarsened dendrite, we can reproduce the so-called ''doublon'' formation previously found in direct numerical simulations with surface energy using the quasi-stationary approximation [51] and fully unsteady equations [52]. Using the initial conditions

$$E_{j\,\text{wave1}}=E_{j\,\text{wave2}}=\pm 0.05, \quad t_{1j\,\text{wave1}}=j,$$

$$t_{1j\,\text{wave2}}=2.90j+6.80, \quad \xi_{s0j}(t_{1j})_{\text{wave1}}=\pm 2,$$

$$\xi_{s0j}(t_{1j})_{\text{wave2}}=\pm 4.47,$$

$$\zeta_{sj}(0)=i\pm\sqrt{[\xi_{s0j}(t_{1j})-i]^2-2t_{1j}}, \qquad (5.59)$$

we find the formation of doublons due to side-branch tip splitting in Fig. 13. As in side-branch coarsening, doublon formation results from waves of poles approaching the real axis, but this time with comparable residues. Such structures have also been studied theoretically with the inclusion of surface-energy effects [53] though not in the context of singularity dynamics. Doublons are believed to play an important role in the formation of the ''seaweed'' morphology in the absence of anisotropy [52].

E. Pole-trajectory summary

We now present the following picture for pole movement for the $\mathcal{B}=0$ solution, in the small-residue limit. Let the initial conditions E_j and $\zeta_{sj}(0)$ be given so that the pole starts in quadrant IV, for example. While $\eta_{sj}\gg O(\epsilon)$, the pole moves toward the real axis and away from the origin according to Eq. (5.23) and its companion zero ζ_{0j} moves according to Eq. (5.13). The $O(\epsilon)$ correction to the trajectory (5.28) is singular in finite time, which indicates a breakdown in the solution as we approach $\eta_{sj}=O(\epsilon)$. When $\eta_{sj}=O(\epsilon)$, the pole moves according to the implicit solution (5.32). If inequality (5.25) is satisfied, the pole's companion zero will not hit the axis and the pole's trajectory alters so

that its ξ velocity is the same sign as $\mathrm{Re}(E_j)$, by which time $\eta_{sj} = o(\epsilon)$. Then, the pole's motion is given by Eq. (5.37). Now, recalling that we are still in quadrant IV, if $\mathrm{Re}(E_j) > 0$, satisfying Eq. (5.39), then the pole will continue to move toward $\xi = +\infty$ without further incident, at least until surface-energy effects become important. As it nears the real axis, the pole creates an indentation in the crystal-melt interface that is oriented at an angle $\theta = \tan^{-1}[-\mathrm{Re}(E_j)/\mathrm{Im}(E_j)]$ with respect to the y axis. On the other hand, if $\mathrm{Re}(E_j) < 0$, violating Eq. (5.39), then the pole will be heading toward $\xi = -\infty$, but along the way it will have to cross the imaginary axis. When the pole crosses the imaginary axis, the indentation will cross the tip; a tip splitting will occur and the new tip will outrun the original tip. If at any time a zero is about to hit the real axis [because Eq. (5.25) is violated], the singularities' movements are governed by Eq. (5.48). However, the global effects of cusp formation occur too late in the formation process for there to be much of a global effect before a cusp forms and the $\mathcal{B} = 0$ solution ceases to have meaning.

We also found that there is a correspondence between the small-residue theory and a large-ζ_s theory with well-separated poles. In a generic initial condition consisting of a random distribution of singularities, the singularities would not usually be well separated. This is a limitation of the current large-ζ_s theory, but the theory is still useful for investigating the evolution of a special initial condition consisting of a single pole, or something similar.

We then integrated the poles' equations numerically. We found excellent agreement between the numerical and asymptotic results. We also generated initial conditions for the numerical solutions using the small-ϵ theory so that we could control the final form of the crystal-melt interface. Three generic types of behavior of the zero-surface-energy solutions include dendritic behavior, tip splitting, and cusp formation. Numerically, we only looked at examples of the interface behavior. A more ambitious numerical investigation would be to look at the evolution of the interface with random distributions of singularities (since we are using singularities to simulate random initial noise) and perform some statistical analysis on the dendrite shapes to learn the ''average'' pattern of growth.

Finally, we developed a scenario for side-branch coarsening, in which coarsening is due to the interaction of weaker and stronger poles. The weaker poles create narrow indentations in the crystal-melt interface and then the stronger poles create wider indentations that stop the growth of the narrow sidebranches. We caution that these pole interactions may not be the only mechanism leading to side-branch coarsening. Furthermore, without surface-energy effects, there is no determination of the various length scales and angle selections present in real dendrites.

VI. CONCLUSION

We have considered time-evolving aspects of a one-sided two-dimensional model for dendritic crystal growth for small undercooling (i.e., Péclet number $P \ll 1$). We have identified a large region (I) around the tip where the temperature field is harmonic. When the initial interfacial and temperature deviations from the Ivantsov solution are limited to this region,

we show that it is consistent to assume that the solution in other far-field asymptotic regions is given by the Ivantsov solution for $t \ll P^{-1}$.

Within this interval of time, we considered various aspects of both linear and nonlinear dynamics in region I. We have obtained expressions for the linear growth of an arbitrary short-wavelength disturbance about an arbitrarily time-evolving base state, not necessarily steady. Concrete expressions have been obtained for large times in the restricted case for which the base state approaches an Ivantsov parabola in the far field. These expressions are in agreement (up to a prefactor) with those obtained by Barber, Barbieri, and Langer [16] for a globally steady base state. We also show that linear theory predicts that an initially localized disturbance does not remain localized: a fact that does not seem to have been recognized before. Further, in this case, the growth of disturbances is related to the zero-surface-energy motion of singularities. The dispersion of such a disturbance into a partially wavy interface with a sharp edge is related to the Stokes phenomenon exhibited by the solution of the inner equations governing the region in which small surface-energy effects become important.

With the connection of zero-surface-energy singularity motion to interfacial dynamics for small, nonzero surface energy exemplified in the linear problem, we examined as fully as possible, in Sec. IV and later, the nonlinear dynamics of the zero-surface-energy singularity motion. This approach serves as a starting point for inclusion of small surface-energy effects, planned to be shown in future papers. We studied various features of the nonlinear dynamics of complex singularities in the lower-half complex ζ plane that are relevant to finger competition, cusp formation, and side-branching. However, not all the features of the zero-surface-energy dynamics are relevant in the limit of zero-surface energy, as we plan to demonstrate for a specific set of initial conditions in future papers. Nonetheless, the relation between singularity motion and localized disturbance dynamics transcends the restrictions of linear analysis. Changes in motion of zero-surface-energy complex singularities due to nonlinear effects have immediate consequences for the growth of interfacial disturbances, even with small but nonzero surface-energy effects. In particular, our findings on the motion of pole singularities imply that the maximal growth rate of a general disturbance advecting far from the tip will not be proportional to the linear growth $\exp[c(-y_d)^{1/4}]$, where y_d is the y location (Fig. 1) of the center of the disturbance and c is some constant depending on surface energy. Instead, nonlinear theory for disturbances associated with poles gives rise to an associated conformal map growing as $\exp[c(-y_d)^{1/2}]$ and the interfacial disturbance remains localized, contrary to linear theory predictions. The dependence of the constant c on surface energy is not addressed here. Further, for a localized disturbance associated with a pole close the real axis in the lower-half plane, there is no dispersion, in contrast with the predictions of linear theory. It is also clear from the nonlinear analysis that unlike the linear case, the growth rate, as well as other features of the disturbance, is not independent of the type of complex singularities associated with it.

We have also given a scenario for dendrite coarsening in terms of the motion of complex singularities. At this stage, this is only a scenario rather than a complete explanation

since the selection effects of surface energy is missing from our analysis thus far. Inclusion of surface energy is necessary for developing concrete predictions of the coarsening rate.

Most of this paper concentrates on the nonlinear aspects of a generally time-evolving dendrite problem; as far as we know, this is the first analytical calculation of its kind. The method is based on studying dynamics in the complex plane, where the zero-surface-energy problem is well posed. Such an approach allows investigation of small nonzero surface energy effects by means of singular perturbation methods.

Another point to be remembered in comparing interfacial predictions arising from complex singularity dynamics with real experimental data or numerical calculations is that the starting point of our investigation is a particular conformal map, with a specified singularity distribution in the extended complex plane. In experiment or simulation, there is some nonzero error involved in the specification of initial condition (experimental noise or roundoff error). The analytic continuation of such initial conditions will invariably lead to rather different distributions of singularities than what we start out with (unless a filtering procedure similar to Krasny's [54] is employed in simulation). Thus real-life interfacial dynamics is to be understood in terms of the dynamics of an ensemble of initial singularity distributions that leave the interface shape invariant to within experimental error. Our approach explains what would happen only for one specific realization, which must then be complemented with studies of an ensemble of initial states, which would then presumably allow comparison with experiment or simulation (without filtering). Further, the class of initial conditions considered has been restricted to functions that are analytic, but have very specific forms for isolated singularities in the lower-half complex plane. We cannot, for instance, accommodate initial interfacial shapes whose analytic continuation in the complex plane contains natural boundaries, which is to be expected for generic initial conditions. Nonetheless, we believe that the aggregate features of the dynamics should not be be very sensitive to the precise class of initial singularities.

[1] J. S. Langer, *Chance & Matter*, edited by J. Souletie (North-Holland, Amsterdam, 1987).

[2] D. A. Kessler, J. Koplik, and H. Levine, Adv. Phys. **37**, 255 (1988).

[3] P. Pelce, *Dynamics of Curved Fronts* (Academic, New York, 1988).

[4] M. E. Glicksman and S. P. Marsh, in *Handbook of Crystal Growth*, edited by D. T. J. Hurle (North-Holland, Amsterdam, 1993), Vol. 1.

[5] W. W. Mullins and R. F. Sekerka, J. Appl. Phys. **34**, 323 (1963).

[6] G. P. Ivantsov, Dokl. Acad. Nauk SSSR **58**, 569 (1949).

[7] G. Horvay and J. Cahn, Acta Metall. **29**, 717 (1961).

[8] S. C. Huang and M. E. Glicksman, Acta Metall. **29**, 701 (1981).

[9] M. E. Glicksman (unpublished).

[10] J. S. Langer and H. Muller-Krumbhaar, J. Cryst. Growth **42**, 11 (1977).

[11] R. Brower, D. Kessler, and H. Levine, Phys. Rev. Lett. **51**, 1111 (1983); E. BenJacob, N. Goldenfeld, J. S. Langer, and G. Schon, *ibid.* **51**, 1930 (1983).

[12] D. Kessler, J. Koplik, and H. Levine, Phys. Rev. A **33**, 3352 (1986); D. Meiron, *ibid.* **33**, 2704 (1986); M. BenAmar and B. Moussallam, Physica D **25**, 155 (1987); A. Barbieri, D. Hong, and J. Langer, Phys. Rev. A **35**, 1802 (1986); M. BenAmar, Y. Pomeau, Europhys. Lett. **2**, 307 (1986); M. BenAmar, Physica D **31**, 409 (1988); S. Tanveer, Phys. Rev. A **40**, 4756 (1989).

[13] D. Kessler and H. Levine, Phys. Rev. Lett. **57**, 3069 (1986); E. Brener and V. I. Melnikov, J. Phys. (Paris), Colloq. **51**, 157 (1990).

[14] E. Brener and V. I. Melnikov, Adv. Phys. **40**, 53 (1991); M. BenAmar and E. Brenner, Phys. Rev. Lett. **71**, 589 (1993); E. Brenner, *ibid.* **71**, 3653 (1993).

[15] R. Pieters and J. S. Langer, Phys. Rev. Lett. **56**, 1948 (1986).

[16] M. Barber, A. Barbieri, and J. S. Langer, Phys. Rev. A **36**, 3340 (1987).

[17] D. A. Kessler and H. Levine, Europhys. Lett. **4**, 215 (1987).

[18] B. Caroli, C. Caroli, and B. Roulet, J. Phys. (Paris), Colloq. **48**, 1423 (1987).

[19] J. A. Sethian and J. Strain, J. Comput. Phys. **98**, 231 (1992).

[20] J.M. Sullivan,Jr.D. R. Lynch, and K. O. Neill, J. Comput. Phys. **69**, 81 (1987).

[21] Damir Juric and G. Trygvasson, J. Comput. Phys. **123**, 127 (1996).

[22] R. Almgren, J. Comput. Phys. **106**, 337 (1993).

[23] K. Brattkus and D. I. Meiron, SIAM (Soc. Ind. Appl. Math.) J. Appl. Math. **52**, 1303 (1992).

[24] J. S. Langer, in *Directions in Condensed Matter Physics*, edited by G. Grinstein and G. Mazenko (World Scientific, Singapore, 1986).

[25] G. Fix, in *Free Boundary Problems*, edited by A. Fasano and M. Primocerio (Pitman, London, 1983), p. 580.

[26] G. Caginalp, in *Free Boundary Problems Involving Solids*, edited by J. M. Chadam and H. Rasmussen (Longman, Essex, 1993), p. 92.

[27] G. Caginalp and E. A. Socolovsky, J. Comput. Phys. **95**, 85 (1991).

[28] R. Kobyashi, Physica D **63**, 410 (1993).

[29] R. J. Braun, G. B. McFadden, and S. R. Coriell, Phys. Rev. E **49**, 4336 (1994).

[30] A. A. Wheeler, B. T. Murray, and R. J. Schaefer, Physica D **66**, 243 (1993).

[31] R. Almgren, W. Dai, and V. Hakim, Phys. Rev. Lett. **71**, 3461 (1993).

[32] C. Misbah, J. Phys. (Paris), Colloq. **48**, 1265 (1987).

[33] S. Howison, J. Fluid Mech. **167**, 439 (1986).

[34] S. Tanveer, Philos. Trans. R. Soc. London, Ser. A **343**, 155 (1993).

[35] M. Siegel and S. Tanveer, Phys. Rev. Lett. **56**, 419 (1995).

[36] M. Siegel, S. Tanveer, and W. Dai, J. Fluid Mech. (to be published).

[37] G. R. Baker, M. Siegel, and S. Tanveer, J. Comput. Phys. **120**, 348 (1995).

[38] G. Caginalp, Ann. Phys. (N.Y.) **172**, 136 (1986).

[39] C. W. Park and G. M. Homsy, J. Fluid Mech. **139**, 291 (1985); D. A. Reinelt, *ibid.* **183**, 219 (1987); S. Tanveer, Philos. Trans. R. Soc. London, Ser. A **354**, 1065 (1996).

[40] R. Churchill and J. Brown, *Complex Variables and Applications* (McGraw-Hill, New York, 1984).

[41] D. A. Kessler and H. Levine, Europhys. Lett. **4**, 215 (1987).

[42] G. F. Carrier, M. Krook, and G. E. Pearson, *Functions of a Complex Variable* (Hod, Ithaca, 1983).

[43] A. A. Lacey, J. Aust. Math. Soc. B, **24**, 171 (1982).

[44] L. A. Galin, Dokl. Akad. Nauk SSSR **47**, 246 (1945).

[45] P. Ya Polubarinova-Kochina, Dokl. Akad. Nauk SSSR **47**, 254 (1945).

[46] P. G. Saffman, Q. J. Math. . **12**, 146 (1959).

[47] B. Shraiman and D. Bensimon, Phys. Rev. A **30**, 2840 (1985).

[48] R. Burlirsch and J. Stoer, Numer. Math. **8**, 1 (1966).

[49] E. Hairer, S. Norsett, and G. Wanner, *Solving Ordinary Differential Equations I* (Springer-Verlag, New York, 1993).

[50] M. D. Kunka, Ph.D. dissertation, The Ohio State University, 1995 (unpublished).

[51] E. Brenner, H. Muller-Krumbhaar, Y. Saito, and D. Temkin, Phys. Rev. E **47**, 1151 (1993).

[52] T. Ihle and H. Muller-Krumbhaar, Phys. Rev. E **49**, 2972 (1994).

[53] M. BenAmar and E. Brenner, Phys. Rev. Lett. **75**, 561 (1995).

[54] R. Krasny, J. Fluid Mech. **167**, 65 (1986).